CAPITAL UNIVERSITY OF SCIENCE AND TECHNOLOGY, ISLAMABAD

In Silico Evaluation of *Withania somnifera* Phytochemicals for Targeting Key Proteins in Gallbladder Cancer

by

Aqsa Batool

A thesis submitted in partial fulfillment for the degree of Master of Science

in the

Faculty of Health and Life Sciences
Department of Bioinformatics and Biosciences

2026

CERTIFICATE OF APPROVAL

In Silico Evaluation of *Withania somnifera* Phytochemicals for Targeting Key Proteins in Gallbladder Cancer

by

Aqsa Batool

(MBS243016)

THESIS EXAMINING COMMITTEE

S. No.	Examiner	Name	Organization
(a)	External Examiner	Dr. Rehana Rani	Abasyn Uni., Islamabad
(b)	Internal Examiner	Dr. Sohail Ahmad Jan	CUST, Islamabad

Dr. Erum Dilshad
Thesis Supervisor
April, 2026

Dr. Syeda Marriam Bakhtiar
Head
Dept. of Bioinfo. and Biosciences
April, 2026

Dr. Sahar Fazal
Dean
Faculty of Health and Life Sciences
April, 2026

Author's Declaration

I, **Aqsa Batool** hereby state that my MS thesis titled "***In Silico* Evaluation of *Withania somnifera* Phytochemicals for Targeting Key Proteins in Gallbladder Cancer**" is my own work and has not been submitted previously by me for taking any degree from Capital University of Science and Technology, Islamabad or anywhere else in the country/abroad.

At any time if my statement is found to be incorrect even after my graduation, the University has the right to withdraw my MS Degree.

(Aqsa Batool)

Registration No: MBS243016

Plagiarism Undertaking

I solemnly declare that research work presented in this thesis titled "***In Silico* Evaluation of *Withania somnifera* Phytochemicals for Targeting Key Proteins in Gallbladder Cancer**" is solely my research work with no significant contribution from any other person. Small contribution/help wherever taken has been duly acknowledged and that complete thesis has been written by me.

I understand the zero tolerance policy of the HEC and Capital University of Science and Technology towards plagiarism. Therefore, I as an author of the above titled thesis declare that no portion of my thesis has been plagiarized and any material used as reference is properly referred/cited.

I undertake that if I am found guilty of any formal plagiarism in the above titled thesis even after award of MS Degree, the University reserves the right to withdraw/revoke my MS degree and that HEC and the University have the right to publish my name on the HEC/University website on which names of students are placed who submitted plagiarized work.

(Aqsa Batool)

Registration No: MBS243016

Acknowledgement

First and foremost, I express my deepest gratitude to Allah Almighty for granting me the strength, wisdom, perseverance, and clarity of thought required to successfully complete this research work. His blessings enabled me to overcome challenges and remain steadfast throughout this academic journey. I would like to extend my sincere and profound gratitude to my supervisor, Dr. Erum Dilshad, for her invaluable guidance, constant encouragement, and constructive feedback throughout all stages of this research. Her academic insight, mentorship, and unwavering support played a pivotal role in shaping this work and enhancing my research skills. I am also extremely thankful to the respected examiners for their time, critical evaluation, and insightful suggestions, which made my thesis defense a meaningful learning experience and contributed significantly to improving the quality of this work. Furthermore, I acknowledge and appreciate the support of all faculty members and staff of the department, as well as the Dean and the Head of Department, for providing a conducive academic environment and the necessary resources to facilitate this research. I would also like to extend my gratitude to my colleague Sarmad Ali for providing technical assistance in the formatting of this thesis. Last but not least, I express my profound gratitude to my parents for their unconditional love, prayers, patience, and continuous moral support, which remained a constant source of motivation throughout this academic endeavor.

(Aqsa Batool)

Abstract

Gallbladder cancer (GBC) is a highly aggressive malignancy characterized by late diagnosis, poor prognosis, and limited therapeutic options, particularly in advanced stages. Conventional chemotherapy, including gemcitabine-based regimens, is associated with systemic toxicity, high cost, and limited long-term efficacy. Therefore, the identification of safer and more targeted therapeutic alternatives remains a critical need. The present study aimed to identify potential TP53-modulating phytochemicals from Withania somnifera using an integrated computational approach. Six phytoconstituents were selected through literature mining and subjected to molecular docking against TP53, a tumor suppressor protein frequently implicated in gallbladder cancer progression. Drug-likeness screening was performed using Lipinski's Rule of Five, and pharmacokinetic and toxicity properties were evaluated through ADMET analysis using the pkCSM server. Molecular docking was conducted using AutoDock Vina, and protein-ligand interactions were analyzed using PyMOL. Among the screened phytochemicals, withanolide F exhibited the highest binding affinity (-9.265 kcal/mol); however, withanolide E demonstrated a favorable balance between binding affinity (-8.316 kcal/mol), physicochemical suitability, and pharmacokinetic properties. Withanolide E showed excellent predicted intestinal absorption (100%), favorable volume of distribution (0.093 log L/kg), moderate total clearance (0.378 log mL/min/kg), and absence of hepatotoxicity and hERG inhibition. Based on this comprehensive evaluation, withanolide E was selected as the lead compound. The selected lead compound was subsequently compared with gemcitabine, an FDA-approved drug for GBC treatment. Although gemcitabine exhibited a stronger binding affinity toward TP53 (-9.333 kcal/mol), it displayed pharmacokinetic limitations, including moderate intestinal absorption, poor membrane permeability, intravenous-only administration, and predicted hepatotoxicity. In contrast, withanolide E demonstrated stable binding at a surface-accessible regulatory region of TP53, consistent with its potential modulatory role. In conclusion, while gemcitabine remains a potent clinical anticancer agent, withanolide E emerges as a promising natural lead compound with superior predicted safety and pharmacokinetic characteristics. It

is recommended that withanolide E undergo further in vitro, in vivo, and molecular dynamics investigations to validate its therapeutic potential for gallbladder cancer management.

Key words: Gallbladder cancer, *Withania somnifera*, Withanolide E, TP53, gemcitabine, Molecular docking

Contents

List of Figures

List of Tables

Abbreviations

ADMET	Absorption, distribution, metabolism, excretion, and toxicity
APBDJ	Abnormal Pancreaticobiliary Duct Junction
BTC	Biliary tract cancer
COSMIC	Catalogue of Somatic Mutations in Cancer
GC	Gemcitabine + cisplatin
GC-MS	Gas chromatography–mass spectrometry
GBC	Gallbladder cancer
HCC	Hepatocellular carcinoma
HER2/ERBB2	Human epidermal growth factor receptor 2
FHIT	Fragile histidine triad
KRAS	Kirsten rat sarcoma viral oncogene homolog
LC-MS	Liquid chromatography–mass spectrometry
NMR	Nuclear Magnetic Resonance
OS	Overall survival
PDB	Protein Data Bank
PD-1	Programmed cell death protein 1
PD-L1	Programmed death-ligand 1
PFS	Progression-free survival
SEMA3B	Semaphorin 3B
TP53	Tumor protein 53
WA	Withaferin A
WS	Withanolides (steroidal lactones)

Chapter 1

Introduction

Gallbladder cancer is classified among the deadliest, invasive, and high grade cancers, marked by exceptionally high fatality rate. On a global scale, it is regarded as the most reported cancer of biliary tract, accounting for $\approx 66\%$ of all biliary tract cancer diagnoses. Owing to the advanced stage and poor prognosis, the individuals with Gallbladder cancer have the median survival time of less than one year, 5-year survival rate of about 5%. This poor outcome is a direct consequence of delayed diagnosis, intrinsic malignant nature, narrow treatment scope, and elevated risk of relapse [1]. Lymphatic or hematogenous metastasis and hepatic invasion are the leading causes of early spread of GBC. Patients with a progressive disease state usually do not respond to the surgical and non-surgical treatments, whereas early-stage cases may be cured with surgery [2].

The pathogenesis of GBC is complex, and the molecular pathogenesis of this disease are not yet fully elucidated; however, the disease has been linked to broad range of predisposing environmental factors and genetic variants, including Cholelithiasis, arsenic ingestion, long term *Salmonella typhi* infection, Non-Juvenile diabetes, adiposity, multiple parity specific dietary products, predisposing genetic factors, and consumption of sugary drinks [3].

Furthermore, females are more prone to this disease as compare to the men, mainly due to hormonal imbalance which causes the increase levels of cholesterol in the

bile, eventually leading to the formation of gallstones. By using different approaches of genome wide analysis, multiple genes have been identified as the potential candidates for Gallbladder cancer onset, including KRAS, TP53, and c-ERB-B2. A few ongoing studies are focusing on the other risk factors involve in lipid movement via liver, gallbladder, and bile duct [4]. Adenocarcinoma accounts for more than 90 percent of GBC cases.

This disease can be classified in several subtypes based on histopathology, including papillary, squamous, mucinous, and adeno-squamous carcinomas. Based of differentiation patterns, the most common type is biliary type followed by the intestinal and gastric-foveolar types. Regarding tumor localization, nearly two-thirds of cases arise in the fundus, one-third in the body, and a minor proportion in the neck region of the gallbladder [4]. For early-stage GBC, the most effective treatment is surgery. Depending on the anatomical location of the tumor and preoperative staging accuracy, a suitable surgery approach is being selected, and adherence to surgical criteria leads to achieve optimal outcomes. However, due to poor prognosis, the patient might be diagnosed in the progressive stage where it has been metastasized, making surgery an un-suitable treatment approach. Therefore, there is an urgent need of new treatment plans like neo-adjuvant therapy, adjuvant therapy or, first-line and second-line treatments for advance stage cancer.

Immunotherapies and gene targeted therapies are promising approaches, but there is still no concrete evidence that they significantly improve survival rate [5]. It is essential today to explore new strategies and processes to combat and treat various types of cancer and other disorders. Over the past decade, numerous medicinal herbs have been administered to cancer patients as potential treatments. These plants possess remarkable properties such as anti-fungal, anti-bacterial, anti-cancer, anti-proliferative, and anti-tumor activities. Some of the well-known compounds include vinblastine, vincristine, podophyllotoxin, paclitaxel (Taxol), and camptothecin, which have been tested clinically. Others, such as vinflunine ditartrate, anhydrovinblastine, NK-611, tafluposide, paclitaxel poliglumex, combretastatins, salvicine, curcumin, indirubin, triptolide, and homoharringtonine, are still under clinical trial [6].

Phytochemicals have demonstrated promising potential in cancer prevention and in improving the quality of life of cancer patients since their initial discovery. Unlocking the molecular mechanisms of these effective phytochemicals could revolutionize cancer treatment approaches [7].

Withania somnifera, locally known as Ashwagandha, is a part of Solanaceae family, having wide range of medicinal properties. In Ayurvedic medicinal formulations, Ashwagandha plays a role of core ingredient. About forty years back, a crystalline steroidal compound, withaferin A (WA) was isolated from the leaves of this plant which showed incredible results in treating cancers. The underlying mechanism by which it inhibits metastasis involves the up-regulation of reactive oxygen species (ROS) and BCL-2 protein which eventually induce programmed cell death (Apoptosis) via mitochondria-dependent pathway in various cancers. Withanolides are the most bioactive constituents of WS and demonstrates significant anti-cancer properties along with anti-inflammatory, anti-oxidant, anti-stress, and anti-angiogenic effects [8].

1.1 Problem Statement

Gallbladder cancer (GBC) lacks safe and effective long-term treatment options, necessitating the identification of novel therapeutic agents with improved efficacy and reduced toxicity.

1.2 Hypothesis

The application of medicinal plants is a safer and more economical approach than commercially available drugs that are very expensive or have adverse effects. Natural compounds found in plants have always provided aid in drug discovery and development hence there is search of phytoconstituents for safe and effective treatment for Gallbladder cancer. *Withania somnifera* (Ashwagandha), a medicinal plant known for its anticancer and immunomodulatory properties, has shown potential in inhibiting tumor growth and inducing apoptosis in various cancers.

However, its therapeutic role and underlying molecular mechanisms against gallbladder cancer remain poorly understood. In this context, effectiveness of phytoconstituents of *Withania somnifera* against GBC will be studied.

1.3 Aims and Objectives

The aim of this study is to identify and evaluate plant-based phytochemicals from *Withania somnifera* as potential therapeutic agents against gallbladder cancer using computational approaches. The objectives included:

i. To identify and select bioactive phytochemicals from Withania somnifera relevant to gallbladder cancer treatment through literature mining.

ii. To evaluate the drug-likeness, physicochemical properties, and ADMET profiles of the selected phytochemicals using *in silico* tools.

iii. To perform molecular docking of selected phytochemicals against major GBC-associated targets (TP53, KRAS, and c-ERB-B2/HER2).

iv. To analyze protein–ligand interactions and binding affinities to identify a lead compound and compare it with the approved therapeutic drug used for gallbladder cancer.

Chapter 2

Literature Review

2.1 Gallbladder Cancer

Gallbladder cancer primarily arises from the mucosal epithelium of the gallbladder and is the most common malignant neoplasm of the biliary tract. It is associated with an aggressive clinical course and a poor prognosis [9].

The following sections comprehensively address the epidemiology, anatomical and histopathological characteristics, etiology and risk factors, molecular pathogenesis, current diagnostic and prognostic approaches, as well as existing treatment strategies and their limitations related to gallbladder cancer.

2.1.1 Epidemiology and Global Incidence

Characterized by unfavorable prognosis, Gallbladder Cancer is a life threatening disease. Listed as 23rd most prevalent type of cancer in the world and marked on 6th position in terms of gastrointestinal tract malignancies. On initial stages, it remains asymptomatic. Owing to this, in most of the cases the cancer is either metastasized locally or in distant areas, making it difficult to treat [10]. Due to the uneven global distribution of GBC, regions such as China, the Indian subcontinent, and South America have emerged as major hotspots. Combination of

environmental and genetic factors contributes to this variation. The unequal distribution of GBC is also observed between genders. It mostly affects females leading to the grim outcomes [10]. As reported by the GLOBOCAN 2022 database, total of 122,469 new cases of gallbladder cancer (GBC) and 89,045 associated deaths were reported globally in 2022 (Table 2.1), with China accounting for the highest number of new cases. The global age-standardized incidence and mortality rates were 1.2 and 0.83 per 100,000 populations, respectively [11]. Table 2.1 suggests

TABLE 2.1: New cases and deaths, age-standardized rates (ASR) of incidence and mortality (per 100 000 person-years) of gallbladder cancer by sex and world region, 2022 [11].

World region	Incidence						Mortality					
	Both		Male		Female		Both		Male		Female	
	Cases	ASR	Cases	ASR	Cases	ASR	Cases	ASR	Cases	ASR	Cases	ASR
Eastern Africa	1295	0.57	437	0.43	858	0.69	1112	0.49	370	0.37	742	0.60
Middle Africa	169	0.20	66	0.18	103	0.22	147	0.18	59	0.16	88	0.19
Northern Africa	3086	1.40	1012	0.96	2074	1.80	2207	0.98	726	0.70	1481	1.30
Southern Africa	366	0.61	72	0.27	294	0.87	187	0.33	56	0.23	131	0.40
Western Africa	596	0.28	224	0.24	372	0.31	545	0.26	205	0.23	340	0.29
Caribbean	335	0.53	86	0.30	249	0.73	227	0.36	62	0.21	165	0.50
Central America	1750	0.88	368	0.40	1382	1.30	1182	0.59	290	0.31	892	0.82
South America	8349	1.40	2535	0.92	5814	1.80	5638	0.91	1753	0.63	3885	1.20
Northern America	5229	0.65	1739	0.46	3490	0.83	2453	0.28	811	0.20	1642	0.35
Eastern Asia	46191	1.30	19179	1.20	27012	1.50	34734	0.96	13988	0.85	20746	1.10
South-Eastern Asia	4758	0.61	2237	0.65	2521	0.60	3491	0.45	1628	0.47	1863	0.44
South Central Asia	35266	1.80	10729	1.10	24537	2.40	27227	1.40	8238	0.83	18989	1.90
Western Asia	1897	0.71	682	0.54	1215	0.87	1369	0.51	557	0.45	812	0.58
Eastern Europe	4976	0.75	1438	0.58	3538	0.87	3444	0.51	979	0.39	2465	0.60
Northern Europe	2011	0.70	561	0.41	1450	0.96	1260	0.41	348	0.25	912	0.56
Southern Europe	2806	0.62	1009	0.51	1797	0.71	1827	0.38	663	0.32	1164	0.43
Western Europe	2877	0.48	965	0.37	1912	0.57	1672	0.26	552	0.20	1120	0.32
Australia-New Zealand	443	0.63	158	0.47	285	0.77	257	0.35	86	0.25	171	0.44
Melanesia	83	1.10	38	1.30	45	1.10	70	0.97	32	1.10	38	0.90

that gallbladder cancer exhibits pronounced geographical and gender-based disparities worldwide, with the highest incidence and mortality rates reported in Asia and South America, particularly in Eastern Asia, South-Central Asia, and South America. Females consistently demonstrate higher age-standardized incidence and mortality rates than males across most regions, likely due to a greater prevalence of gallstones and hormonal and metabolic influences. Although regions such as

Africa and Melanesia report lower absolute case numbers, their high mortality-to-incidence ratios indicate late diagnosis and limited healthcare access. In contrast, North America and parts of Europe show comparatively lower incidence and mortality, reflecting better screening and treatment facilities. Overall, the close correspondence between incidence and mortality underscores the aggressive nature of gallbladder cancer and highlights the urgent need for early detection strategies and improved therapeutic interventions, particularly in high-burden regions [11].

2.1.2 Epidemiological Trends of Gallbladder Cancer in Pakistan

Hospital-based studies in Pakistan indicate a relatively low but clinically significant frequency of gallbladder carcinoma. A five-year retrospective study conducted at Dow Medical College, Karachi (2014–2018), analyzed 948 gallbladder specimens and reported 4 cases of adenocarcinoma, representing a prevalence of 0.42% among all examined samples.

The majority of cases occurred in females, with a mean age of 58 years. Other local studies have reported variable frequencies, ranging from 0.7% to 2.7%, with some data from Karachi suggesting rates as high as 8% in selected populations. These findings highlight regional variability and suggest potential underreporting due to the absence of structured nationwide screening programs in Pakistan. As shown in Figure 2.1, the number of gallbladder cases reached its highest level in 2016 and subsequently declined over the following years [12].

2.1.3 Anatomical and Histopathological Characteristics

This section provides an overview of the normal anatomical structure of the gallbladder and presents a histopathological analysis, highlighting the morphological alterations associated with gallbladder cancer.

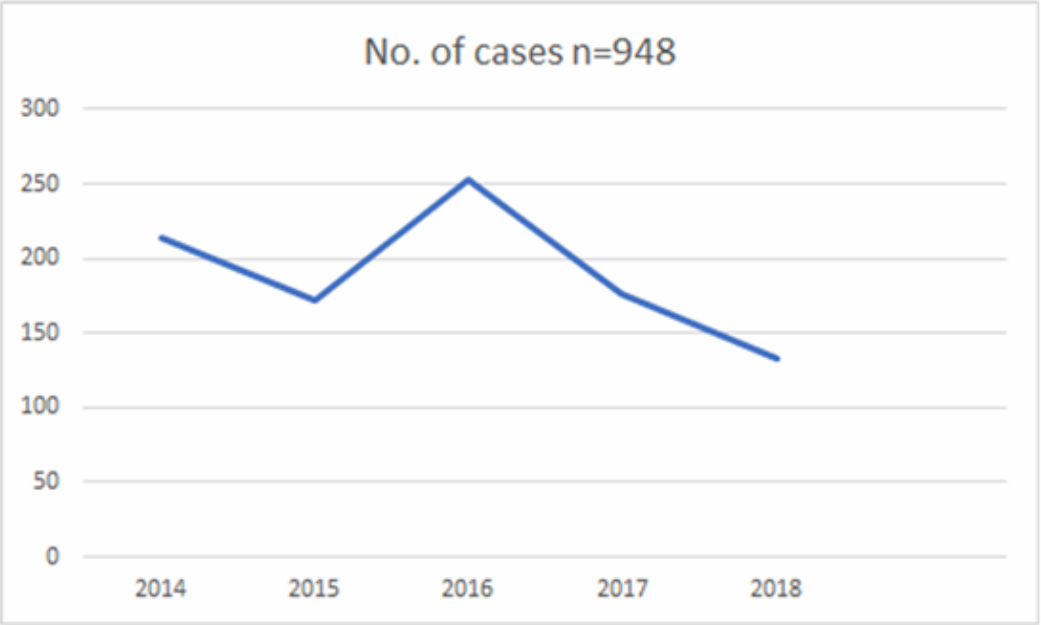

FIGURE 2.1: Annual distribution of gallbladder cases (n = 948) recorded at Dow Medical College, Karachi, from 2014 to 2018, showing a peak in 2016 followed by a gradual decline [12]

2.1.3.1 Structure of Gallbladder

The gallbladder is a pear-shaped organ located just beneath the liver. Its primary function is to store and release bile. It typically measures 7–10 cm in length and 3–5 cm in diameter. In anatomical terms, the gallbladder consists of three main parts, the fundus, body, and neck, which connect to the cystic duct. The wall of the gallbladder is composed of several layers, including the mucosa, epithelium, lamina propria, muscularis, and serosa, as illustrated in Figure 2.2 [13]. A fluid named bile forms in the liver, plays a vital role in the digestion of fats and releasing cholesterol. It is also involving in antimicrobial activities [14].

2.1.3.2 Histopathological Analysis

Gallbladder cancer (GBC) is broadly classified into three main morphological patterns [16]:

i. Mass-replacing: The mass-replacing type represents the most frequently encountered form of GBC. It commonly demonstrates direct invasion into the

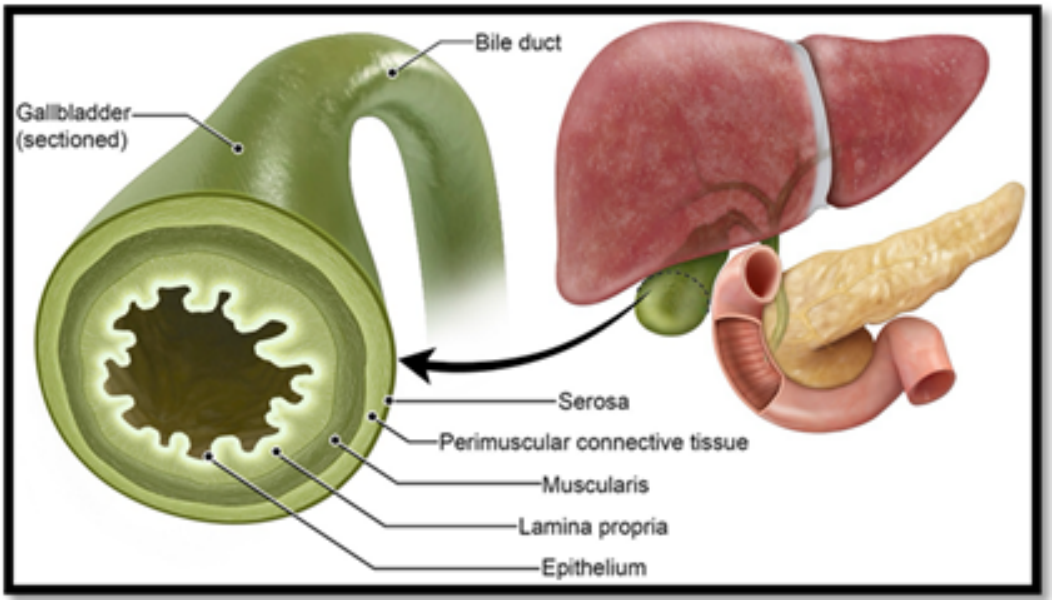

FIGURE 2.2: Anatomy of the Gallbladder and Its Histological Layers [15].

adjacent liver parenchyma and shows a strong propensity for local spread. This type is often associated with biliary obstruction at the porta hepatis and regional lymph node metastasis, reflecting an advanced disease stage at presentation [16].

ii. Wall-thickening: The wall-thickening type poses considerable diagnostic difficulty, as gallbladder wall thickening is a non-specific finding that can be observed in various benign conditions. However, malignant involvement is suggested by asymmetric, irregular, or diffuse wall thickening exhibiting arterial phase enhancement that persists or becomes isodense or isointense relative to the liver during the portal venous phase [16].

iii. Intraluminal polypoidal: The intraluminal polypoidal type accounts for approximately 15-25% of GBC cases and is frequently detected incidentally, as affected patients are often asymptomatic. These lesions are typically confined to the mucosal or muscular layers of the gallbladder and are associated with a relatively favorable prognosis. When identified early, curative treatment with cholecystectomy is often achievable [16].

The most frequently observed form is the mass-replacing form, commonly infiltrates the neighboring liver tissues. The second type remain undiagnosed [16].

According to a case study, histopathology of GBC demonstrates that the epithelial and the mesenchymal components contributes in the tumor formation. As highlighted by the Immunohistochemistry staining, some areas were cytokeratin and CA19.9 positive indicating carcinomatous (epithelial) features. Other areas were vimentin, caldesmon, and SMA positive which is the clear indication of sarcomatous (mesenchymal) features.

Based on the microscopic examination, the dual tissue nature of the tumor was proven because the groups of malignant epithelial cells were enclosed within the malignant mesenchymal tissues. The malignancy of gallbladder is characterized by biphasic composition [17].

2.1.4 Etiology and Risk Factors

A number of genetic factors and environmental exposures are involving in the onset of GBC. The manifestation of GBC is associated with persistent gallbladder infection, certain environmental toxin exposure, or contact with heavy metal or other dietary variables.

Certain evidences suggest that the prevalence of GBC particularly in females and in certain regions of developing nations are associated with various female hormones, cholesterol cycling, and Salmonella infections.

Other predisposing factors include porcelain gallbladder, Mirizzi's syndrome, and pancreatic bile reflux. Some risk factors that can enhance the occurrence of GBC include [18]:

i. Family history of Gallstones

ii. Contact with chemicals

iii. Smoking

iv. Spiked secondary bile acids

v. Fried food items

2.1.4.1 Porcelain Gallbladder

It is an atypical feature of chronic cholecystitis which is marked by the accumulation of the calcium salts on the wall of gallbladder. More than 95% cases are linked with the gallstones. There are around 10% cases of porcelain Gallbladder which are associated with the development of GBC, recent studies show further lower range of 2 to 3%. Greater risks are associated with the localized mucosal or partial wall calcification [18].

2.1.4.2 Gallstones

Gallstones (cholelithiasis) represent the most frequent risk factor for the development of gallbladder cancer (GBC), as approximately 85% of patients diagnosed with GBC have a history of gallstones. However, only about 3% of individuals with gallstones progress to GBC, indicating that additional factors influence malignant transformation.

The risk increases significantly with stone size, and gallstones larger than 3 cm are associated with up to a tenfold higher risk of GBC. Symptomatic gallstones further elevate this risk compared to asymptomatic cases [18]. As illustrated in Figure 2.3, disturbances in cholesterol metabolism, particularly elevated LDL cholesterol levels, increased cholesterol transport, and excessive cholesterol deposition in bile, promote gallstone formation. In contrast, balanced lipid metabolism and bile salt formation reduce stone development. These metabolic alterations create a chronic inflammatory environment in the gallbladder, which may contribute to carcinogenesis [19].

2.1.4.3 Gallbladder Polyps

These are localized growths that emerge on the mucosal linings of the gallbladder. Cholecystectomy or the routine ultrasound examination may lead to its discovery.

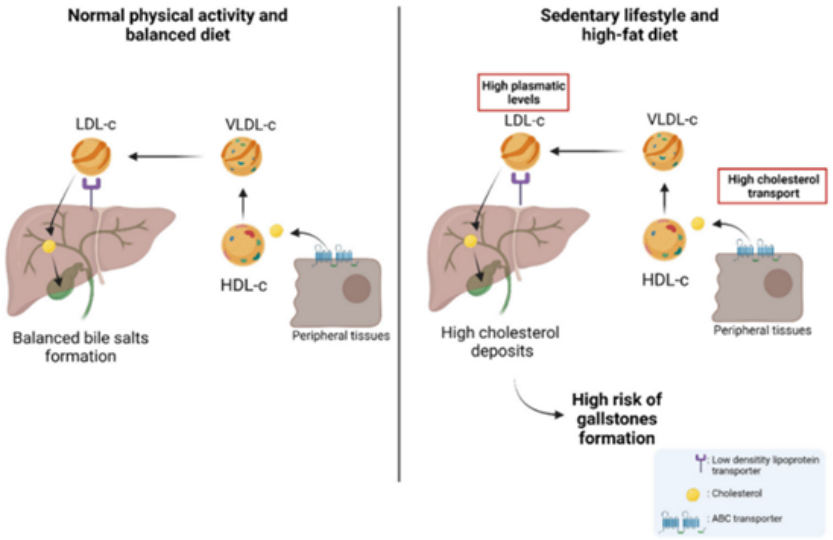

FIGURE 2.3: The cholesterol metabolism and the risk of developing gallstones [19].

Gallbladder polyps have two main categories which are benign and malignant. The benign lesions are further categorized into two sub-types [18]:

i. Neoplastic

ii. Non-neoplastic

One of the most common benign neoplastic lesion is adenoma, characterized by the glandular growth of the cells which mimics biliary system epithelium. Around 5% of the individuals are diagnosed with the polypoid gallbladder lesions which can lead to gallbladder cancer. Patients who have polyps greater than 10 mm have 25% chances of getting GBC [18].

2.1.4.4 Chronic Infection

In Salmonella-endemic regions, approximately 4% of patients with acute Salmonella infection develop chronic infection and become asymptomatic carriers of *Salmonella typhi*. According to various wet lab and *in silico* studies, there is a strong association between chronic *S. typhi* carriage and a heightened risk of developing gallbladder cancer. Gallstone is the leading cause and a potential reservoir for long term infection, as cholelithiasis patients are more prone to become

chronic carriage. Furthermore, Helicobacter species particularly *H. bilis* colonizes the biliary epithelium and plays part in the development of GBC. Advance molecular and immune-histochemical analysis shows the above association is backed by Helicobacter derived toxins and outer membrane proteins. Chronic inflammation resulting from primary sclerosing cholangitis has also been associated with a higher occurrence of gallbladder mass lesions. Consequently, annual gallbladder ultrasound screening is recommended for patients with this condition [18].

2.1.4.5 Congenital Abnormalities

Abnormal dilatations of bile ducts lead to biliary cysts which may be innate or acquired and can emerge singly or in multiples. Choledochal cysts involves only extrahepatic bile duct, but now it also includes intrahepatic cysts. A prevalent situation in Asian population named abnormal pancreaticobiliary duct junction (APBDJ) is exhibited by 70% of the patients with biliary cysts [18]. The risk of developing gallbladder cancer and cholangiocarcinoma, collectively known as biliary malignancies, is significantly increased in individuals with biliary cysts and anomalous pancreaticobiliary duct junctions (APBDJ). The prevalence of cancer is age-dependent, being less than 1% in children and exceeding 50% in adults. APBDJ, characterized by an abnormally long common channel where the pancreatic and bile ducts merge, permits pancreatic juice to reflux into the biliary system, leading to epithelial injury, inflammation, and cyst formation. APBDJ alone, even without the presence of cysts, can elevate the risk of both biliary and pancreatic cancers. Therefore, individuals diagnosed with this anomaly are often advised to undergo prophylactic cholecystectomy [18].

2.1.4.6 Carcinogenic Exposure

According to some studies, environmental and occupational carcinogens exposure lead to the manifestation of gallbladder cancer. Industry workers specifically workers of oil refineries, paper manufacturing industries, chemical manufacturing industries, footwear and textile industries are at greater risks. In addition to this,

miners who are exposed to radon or other radiations are susceptible to GBC. Other deadly factors include smoking, frequent exposure to aflatoxins etc. are the leading case of liver cancer and it may elevate the risk of GBC as well [18].

2.1.4.7 Medication

Certain drugs and treatments have also been linked with elevated risk of emerging biliary cancers [10]:

i. Methyldopa

ii. Oral contraceptives

iii. Menopausal hormone therapies

iv. Isoniazid

2.1.4.8 Body Mass Index and Diabetes

Obesity elevates the likelihood of GBC development. Individual with diabetes mellitus are more prone to GBC as compare to those who do not have diabetes [18].

2.1.5 Molecular Pathogenesis of GBC

Gallbladder cancers (GBCs) most commonly develop in the presence of gallstones and progress through a well-defined sequence of pathological changes, beginning with metaplasia, followed by dysplasia, and ultimately carcinoma. This multistep progression is largely driven by chronic and persistent inflammation, which facilitates malignant transformation and tumor development. These morphological changes are accompanied by the accumulation of genetic and epigenetic alterations that persist and intensify during advanced stages of the disease [20]. This section outlines the molecular pathways and alterations involved in the development and progression of gallbladder cancer.

2.1.5.1 Molecular Pathways

Scientific data suggests that there are two primary mechanisms that are involved in the progression of GBC [21].

i. Frequent inflammation of gallbladder due to gallstones.

ii. Anomalous Pancreaticobiliary Junction (APBJ)

The former one is considered to be the most common pathway for GBC globally while the later one is less common and was predominantly observed in East Asian Populations, particularly in Japan and Korea [21].

Figure 2.4 illustrates the major molecular and pathological pathways involved in the progression of gallbladder cancer. One pathway originates from cholelithiasis, where persistent gallstones induce chronic inflammation of the gallbladder epithelium, leading to genomic instability and inactivation of the tumor suppressor gene TP53. Loss of TP53 function disrupts cell cycle regulation and apoptosis, promoting epithelial dysplasia and eventual carcinoma formation. The second pathway involves anomalous pancreaticobiliary junction (APBJ), which allows reflux of pancreatic enzymes into the biliary tree, causing repeated epithelial injury.

This chronic exposure facilitates oncogenic KRAS mutations, further driving dysplastic changes and malignant transformation. Both pathways converge at dysplasia, highlighting inflammation-driven genetic alterations as key events in gallbladder carcinogenesis (Figure 2.4) [13]. The underlying genetic and molecular pathways for GBC progression are highlighted by these two mechanisms. In the initial stages, GBC is strongly associated with the female gender, the presence of gallstones, and TP53 gene mutations worldwide.

In contrast, APBJ-associated GBC tends to occur at a younger age, shows a lower prevalence in females, and is not related to gallstones. KRAS mutations, along with delayed TP53 mutations, are the characteristic genetic alterations underlying this mechanism [21].

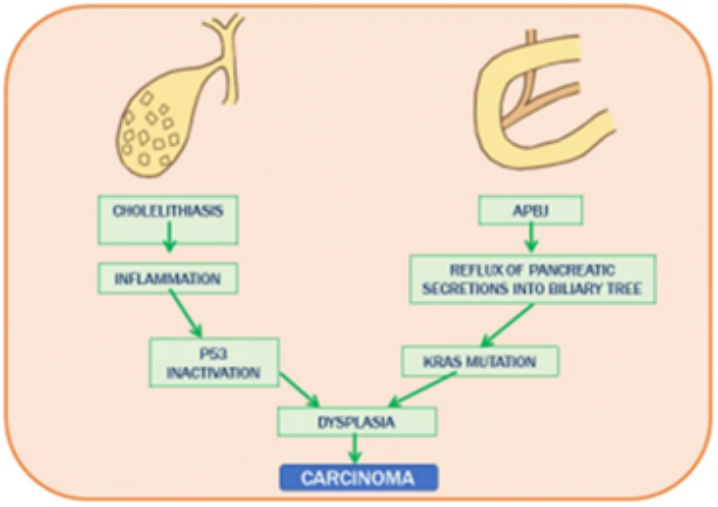

FIGURE 2.4: Pathways of GBC Progression [13].

2.1.5.2 Molecular Changes in GBC

A study reported that the analysis of the Catalogue of Somatic Mutations in Cancer (COSMIC) database indicates that TP53 is the most frequently mutated gene in gallbladder cancer. Other commonly altered genes include ERBB family genes, PI3K–AKT pathway genes, ARID1/2, KRAS, SMAD4, ELF3, and CTNNB1. These mutations collectively contribute to tumor initiation, progression, and poor clinical outcomes [20].

i. TP53 Gene Mutation

   Genomic Integrity is preserved by the essential role of TP53 tumor suppressor Gene. Alteration in this gene can lead to any type of cancer, because this mutation occurs in almost 50% of human cancers. Mutation in TP53 causes uncontrolled proliferation of mutated cells leads to the progression of GBC. Out of 393 codons of TP53 gene, more than 280 codons undergo mutation. The highest frequency of mutation was observed between exon 5 and exon 8. It is one of the most initial mutation in the cancer progression, often occurred when the mucosa still appears normal histologically. This mutation leads to the overexpression of a dysfunctional p53 protein. Nearly half of all TP53 mutations in GBC are found within exon 5, although no distinct mutational "hotspot" has been identified [21].

ii. ERBB Signaling Pathway Alterations

The ERBB signaling pathway represents the most frequently identified driver pathway in GBC. Mutations have been reported in ERBB2 (HER2), ERBB3, ERBB4, and EGFR, which activate downstream oncogenic signaling [20].

(a) Approximately 40% of early-stage GBC tumors exhibit ERBB2 mutations.

(b) One study reported 45.5% ERBB2 mutations, predominantly novel mutations in exon 21.

(c) ERBB4 mutations were observed in 21.2% of cases.

(d) EGFR mutations were present in 24.2% of patients.

iii. Mitochondrial DNA Mutations

Due to chronic inflammation, level of ROS increases which causes damage in the cell ultimately leads to mutations in the mitochondrial DNA. The most prevalent mutation, the mtDNA D310 alteration, has also been recognized as an early stage in the pathogenesis of GBC. Like TP53 mutations, mitochondrial DNA–mutated cells typically display no apparent histological abnormalities. Given that both chronic cholecystitis and gallbladder cancer share comparable genetic alterations, it is likely that a common underlying inflammatory process drives the development of both conditions [21].

iv. Fragile Histidine Triad Gene Mutation

In Gallbladder cancer analysis, it was identified that Tumor suppressor genes such as SEMA3B and Fragile Histidine Triad (FHIT) are inactivated via epigenetic mutations. Suppression of FHIT expression leads to the chronic cholecystitis-linked GBC, implying that genetic instability is promoted by the frequent inflammation. Over-expression of TP53 and loss of FHIT were observed in the adjacent mucosa of GBC lesions, implying the idea that tumorigenesis begins long before histological malignancy becomes evident [22].

v. Proto-oncogene KRAS Mutations Gallbladder cancer linked with abnormal pancreaticobiliary duct junction (APBJ) than those related to cholelithiasis

are characterized by the mutations in the KRAS oncogene [22]. These mutations eventually lead to the activation of downstream signaling pathways such as MAPK and PI3K/AKT, promoting uncontrolled progression.

In accordance with some studies from Japan, it was reported that the APBJ-related GBCs have KRAS mutation rates ranging between 50-80%, as compare to the western population where its frequency is very low [23]. Codon 12 is the most frequently mutated codon, linking with initial carcinogenic changes occurs due to the reflux of pancreatic enzymes into the biliary tract [24].

2.1.6 Current Diagnostic and Prognostic Approaches

Current diagnostic and prognostic approaches for gallbladder cancer are discussed, highlighting commonly used clinical, imaging, and molecular assessment strategies.

2.1.6.1 Hematological Biomarkers

As evidenced by the recent studies, systemic inflammation in gallbladder cancer is diagnosed via following:

i. Neutrophil-to-Lymphocyte Ratio (NLR)

ii. Platelet-to-Lymphocyte Ratio (PLR)

iii. Monocyte-to-Lymphocyte Ratio (MLR)

These diagnostic indicators are accessible and cost-effective. An advance malignancy microenvironment is characterized by the elevated levels of NLR and PLR, while MLR is designated to be a potential independent prognostic marker for overall survival in cancer patients [25].

2.1.6.2 Inflammatory Ratios and Clinical Correlations

Research has shown that hematological ratios and liver enzyme (SGPT, SGOT, ALP, bilirubin) levels are in a significant association. This implies that the systemic inflammation induced by tumor is mainly due to the imbalances in the immune cells. In addition to this, patients from side areas who have inadequate access to healthcare have higher frequency of inflammations, linking socioeconomic and demographic variables to disease prognosis [25].

2.1.6.3 Prognostic Value of NLR, PLR and MLR

In gallbladder cancer patients, poor overall survival rate is predicted by the elevated NLR and MLR values. In contrast, across demographic groups PLR demonstrates inconsistent prognostic reliability. These diagnostic markers help in risk stratification, guiding clinicians in identifying patients at advanced stages or requiring aggressive management [25].

IV. Imaging Techniques Gallbladder cancer can be diagnosed and detected in the early stage using imaging techniques. The thickening of the gallbladder wall is the key indicator of cell proliferation. It could be identified by using ultrasound which is the first prognostic technique and it is readily available and highly effective. In addition to this, benign tumors and malignancy can be differentiated by using more precise diagnostic technique i.e. high-frame-rate-contrast-enhanced ultrasound.

Further advance techniques are available for higher spatial resolution, comprehensive anatomical visualization, wall-thickening type GBC, etc. which are computed tomography (CT) and magnetic resonance imaging (MRI). Moreover, deep learning algorithms along with ultrasound imaging has proven to enhance diagnostic accuracy. Moreover, the integration of deep learning algorithms with ultrasound imaging has demonstrated potential to boost diagnostic accuracy, indicating a promising avenue for future research. Collectively, these imaging techniques facilitate thorough and early detection of gallbladder cancer (GBC) [26].

2.1.7 Existing Treatment Strategies and their Limitations

Existing treatment strategies for gallbladder cancer and their associated limitations are as follows, with an emphasis on therapeutic efficacy, challenges, and clinical outcomes.

2.1.7.1 Surgical Treatment Strategies

Surgical resection remains the cornerstone and most effective treatment for early-stage gallbladder cancer (GBC), aiming for complete tumor removal with clear margins. This often requires extensive procedures, including partial liver resection and lymph node dissection.

Unfortunately, most patients present with advanced disease, making surgical intervention unfeasible and limiting its curative potential. Moreover, even after radical surgery, recurrence rates remain high, approximately 60–70%, and the overall 5-year survival rate remains poor, ranging between 5% and 15% [27].

2.1.7.2 Chemotherapy

For patients with unresectable, advanced, or metastatic gallbladder cancer (GBC), chemotherapy, particularly the gemcitabine–cisplatin (GC) regimen, remains the standard first-line treatment. Although this combination can provide short-term survival benefits, its long-term effectiveness is limited due to the high molecular heterogeneity of GBC and the development of intrinsic chemoresistance.

Cytotoxic agents act by inducing DNA damage during cell replication; however, their therapeutic response differs significantly among individuals. Furthermore, the considerable systemic toxicity associated with chemotherapy restricts its broader clinical utility [27].

2.1.7.3 Targeted Therapy and Immunotherapy

Recent progress in molecular profiling has revealed potential therapeutic targets such as EGFR, HER2, and PD-1/PD-L1, paving the way for targeted therapies and immunotherapeutic approaches.

However, their clinical efficacy remains limited, largely due to the biological heterogeneity of GBC and the absence of large-scale, disease-specific clinical trials. While preliminary findings and ongoing research demonstrate encouraging outcomes, the effectiveness of immune checkpoint inhibitors and targeted drugs has yet to surpass that of conventional chemotherapy, and their incorporation into standard treatment protocols is still being evaluated [27].

2.2 Medicinal Plants in Cancer Therapy

Medicinal plants are regarded as the most primitive known form of medication around the globe since ancient times. Within human communities, factual knowledge of their beneficial effects has been passed down through generations [5].

2.2.1 Historical Perspective of Plant-Based Medicines

Medicinal plants are regarded as the most primitive known form of medication around the globe since ancient times. Within human communities, factual knowledge of their beneficial effects has been passed down through generations [5]. Medicinal plants are considered as the essential part of indigenous medical system in Indian subcontinent particularly Ayurveda, Unani, and, Siddha. These systems have more comprehensive approach towards health, employing remedial properties of plants.

The balance between the mind, body, and soul plays an integral role in these medical systems along with the frequent use of herbs for treatments [28]. Plant extracts have been extensively investigated for their anticancer potential, with

numerous in vitro and in vivo studies conducted against various cancer cell lines. Selected examples of such therapeutic effects are summarized in Table 2.2 [29].

TABLE 2.2: Therapeutic effects of plant extracts on selected cancer cell lines [30–37].

Plant	**Extract/isolate**	**Cancer type**	**Cell line**	**Effects**	**Ref.**
Aristolochia baetica	Hexane, chloroform, and ethyl acetate extracts	Breast	MCF-7	Antiproliferation	[31]
Aristolochia baetica	Methanol extract	Urinary bladder	T-24	Antiproliferation	[31]
Aristolochia baetica	Methanol extract	Colon	HT-29	Antiproliferation	[31]
Aristolochia baetica	Methanol extract	Liver	HepG2	Antiproliferation	[31]
Artemisia annua	Ethanol/water extract	Gastric	HeLa	Inhibition of cell growth	[38]
Artemisia annua	Extract and acetonitrile maceration	Breast	MDA-MB-231	Cytotoxicity; antitumour activity; antiapoptotic effects in vivo	[33]
Artemisia annua	Extract and acetonitrile maceration	Pancreas	MIA-PaCa-2	Cytotoxicity	[33]
Artemisia annua	Extract and acetonitrile maceration	Prostate	PC-3	Cytotoxicity	[33]
Artemisia annua	Extract and acetonitrile maceration	Lung	A549	Cytotoxicity	[33]
Coptidis rhizoma	Aqueous extract	Hepatocellular carcinoma	HepG2; MHCC97-L	Inactivation of eEF2; downregulation of VEGF; suppression of angiogenesis	[34]
Coptidis rhizoma	Extract powder	Esophageal	YES-2	Downregulation of tumour IL-6; anticachectic activity	[35]
Fagonia indica	Steroidal saponin glycoside	Breast	MDA-MB-68	PARP cleavage; caspase-3 cleavage; DNA fragmentation; apoptosis	[36]
Fagonia indica	Aqueous extract	Colon	Caco-2	PARP cleavage; caspase-3 cleavage; DNA fragmentation; apoptosis	[36]
Morus alba	Methanol extract	Colorectal	SW80	ROS- and GSK3β-dependent ATF3 activation; cyclin D1 proteasomal degradation	[37]
Platycodon grandiflorus	Water/ethanol extract	Ovarian	SKOV-3	Downregulation of Bcl-2; upregulation of Bax; caspase activation and mitochondrial cytochrome *c* release	[39]

2.2.2 Phytochemicals as Anticancer Agents

The medicines based on plants have very less side effects and it's because of the reason that human consume diet which has similar chemical compounds that induce tolerance ability. The anti-cancer properties are found in some of the secondary

metabolites of plants such as flavonoids, terpenoids, alkaloids, tannins etc. These compounds stimulate some signaling pathways that alter the proliferations of cells and induce apoptosis in cancerous cells through different biological mechanisms [29]. Many desirable drugs are sourced from natural products. At present, in pharmacotherapy, various modern drugs are derived from ancient medicinal plants. While studying the bioactive molecules of plants, the most essential step is the extraction process. However, extraction techniques are now being modernized through the utilization of ultrasound and supercritical fluid extraction methods. Phytochemical analysis is further supported by advancements in tools and techniques, such as the use of high-performance liquid chromatography (HPLC) and liquid chromatography/mass spectrometry (LC/MS), which have made quantitative and qualitative assessments much easier [5].

2.3 Withania Somnifera - Ashwagandha

In Ayurveda, Ashwagandha is an important herb, also known as "Indian ginseng" or "Winter Cherry" [39]. It is popular for its diverse health benefits including stress and anxiety management, enhancing cognitive function, boosting stamina and strength. Traditional medicine utilizes the roots and berries of the plant. The plant is safe to consume for short period of time, and for long term usage more research is needed. Commercially, it is available in different forms, such as, capsules, powder, and tablet [40].

2.3.1 History of Ashwagandha

Ashwagandha has been in use for thousands of years in Ayurvedic medicine, a 3000 years old system of medication. Charaka Samhita and the Sushruta Samhita, an Indian text, narrates the use of this plant as "rasayana" which means a collection of herbs promoting overall health and long life of humans [40]. Ashwaganda is the most commonly used name, derived from the Sanskrit words "ashva" meaning horse, and "ghanda" meaning smell, indicating a unique smell of this plant and

referring to the faith that it will provide the strength of a horse [39]. It also has anti-oxidant and anti-inflammatory properties, which helps to improve overall brain health [40].

2.3.2 Taxonomical Classification of Ashwagandha

Withania somnifera, commonly known as ashwagandha, is a part of Solanaceae family characterized by green or gray-green leaves, cluster of small and greenish-yellow flowers. Fruit of this plant is red or orange-red berries that have medicinal implications. The height of this plant is maximum 1-1.5 meters, as it belongs to perennial shrub. The taxonomic classification of *W. somnifera* is summarized in Table 2.3 [40].

TABLE 2.3: Taxonomic classification of *Withania somnifera* [40].

Taxonomic rank	**Classification**
Kingdom	Plantae
Order	Solanales
Family	Solanaceae
Genus	*Withania*
Species	*somnifera*

2.3.3 Growth Requirements

Ashwagandha is an indigenous plant of the dry regions of India, North Africa, and the Middle East. Arid and semi-arid regions are favorable for its growth, and it is tolerant of poor soil conditions as well as drought. It is also cultivated in Nepal, Yemen, and China [40].

2.3.4 Phytochemical Composition

In order to treat various pathological conditions, it is essential to develop new medication through the extraction and characterization of secondary plant metabolites [41]. Identification and isolation of diverse range of phytochemical from *W.*

somnifera is done via chromatographic and spectroscopic analysis including column chromatography, gas chromatography-mass spectroscopy (GC-MS), liquid chromatography-mass spectroscopy (LC-MS), nuclear magnetic resonance (NMR), and X-Ray diffraction studies [41]. *Withania somnifera* contains a wide range of bioactive phytoconstituents, including steroidal lactones (withanolides), alkaloids, flavonoids, steroids, and nitro-compounds. Among these, steroidal lactones such as withaferin A, withanone, and various withanolides are considered the principal pharmacologically active constituents due to their reported anticancer properties. Other classes, including flavonoids and alkaloids, contribute to antioxidant and supportive biological activities. The major classes of phytoconstituents present in *W. somnifera* and their representative compounds are summarized in Figure 2.5 [42].

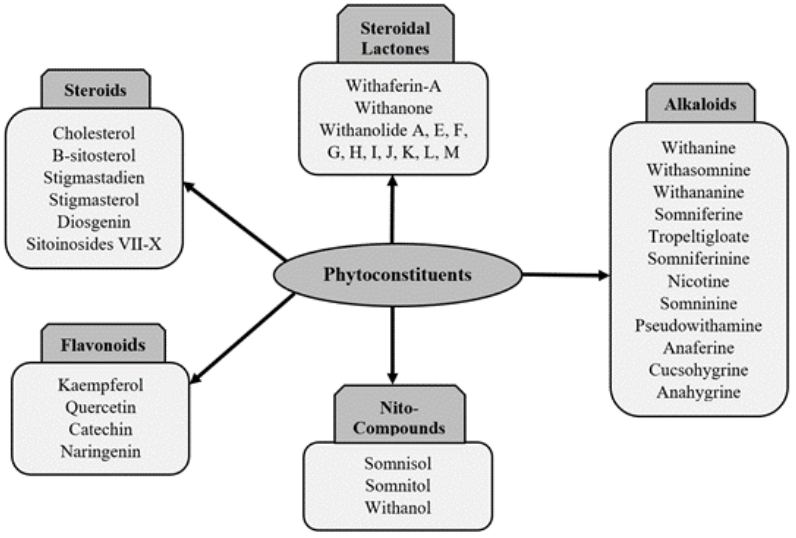

FIGURE 2.5: Pathways of GBC Progression [13].

2.3.5 Molecular Targets of *W. somnifera*

Steroidal lactones known as withanolides (withaferin A and withanolide D) are the core constituent of *W. somnifera*, targeting different biomolecules in the living systems and derives various biological activities. According to various in-vivo and in-vitro experimental studies, target molecules of withaferin A and withanolide D are enzymes such as growth factors, transcription factors, kinases, receptors, and

various structural protein. Withanolides have proven their worth as their therapeutic efficacy is high, specifically against cardiovascular system, cancer, Central Nervous System, inflammation and metabolic disorders as well [42].

As reported in an in-vivo study, there is a powerful suppressive effect in Withaferin A and Withanolide D extracted from the roots of *Withania somnifera* against the inflammatory markers such as IL-2 and IL-8.

Basically it inhibits the proliferation of cancerous cells by inducing apoptosis which results from the upregulation of caspases-3.

Withaferin A follows other mechanisms of suppressing cancer by activating tumor suppressor proteins and the estrogen receptors, so that the intrinsic estrogen would not be able to dock with estrogen receptors [42].

Table 2.4 summarizes the major bioactive phytoconstituents derived from *Withania somnifera*, highlighting their plant source, chemical structures, reported biological activities, and experimental models used for validation. This compilation provides a focused overview of the therapeutic relevance of *W. somnifera* phytochemicals and supports their selection for further mechanistic and computational investigations [42].

2.3.6 Mechanism of Action

Excessive cell division leads to the malignancy which is the characteristic of cancer. *Withania somnifera* has shown remarkable results against malignancy in animal model experimentations and it follows various mechanisms which are as follow [39]

2.3.6.1 NF-$\kappa\beta$ Inhibition

First of all, it blocks the NF-$\kappa\beta$ activation by suppressing the I$\kappa\beta$ kinase β (IKKβ) which activates via TNF. It follows the redox-sensitive thioalkylation mechanism [43].

TABLE 2.4: Description of significant phytoconstituents derived from *W. somnifera* [42].

Phytoconstituent	**Plant part used**	**Compound structure**	**Biological activity**	**Model used**
Withaferin-A	Leaf	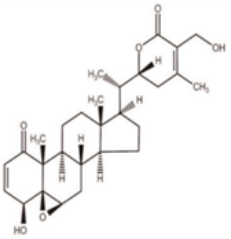	Neuroprotective; Cardioprotective	In-vitro model: C6 glial cell line model; In-vivo: Swiss Albino mice model
Withanone	Fruit	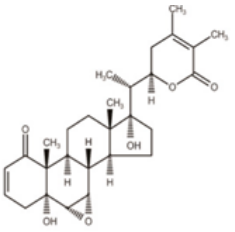	Anti-inflammatory	In-vitro model: LPS-induced bone-derived macrophage
Withanolide-A	Root	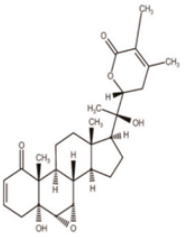	Immunomodulatory	In-vivo model: BALB/c mice model
Withanolide-D	Leaf	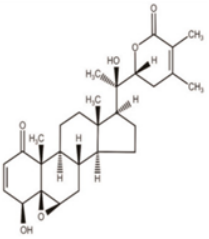	Anti-cancer	In-vivo model: Tumor mice model
Withanolide-E	Leaf	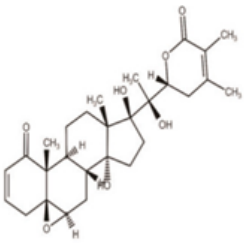	Anti-cancer	In-vivo model: Pancreatic cancer cell lines
Withanolide-F	Leaf	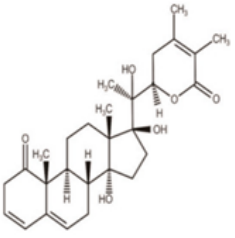	Anti-cancer	In-vivo model: Colon cancer cell lines

2.3.6.2 Tumor Suppressor Activation

Withaferin-A promotes tumor suppressor proteins such as p53 and pRB, which promotes cell cycle arrest and induce apoptosis [43].

2.3.6.3 Death Receptor Pathway

Apoptosis signaling and its triggering is enhanced by the upregulation of the expression of death receptor-5 (DR5) [44].

2.3.6.4 Par-4 and p38 MAPK Activation

Another mechanism for programmed cell death induction is the activation of pro-apoptotic Par-4 and p38 MAP kinase pathways [44].

2.3.6.5 Cell Cycle Arrest

In case of prostate cancer, the levels of phosphorylated Wee-1, histone H3, p21, and aurora B are enhanced, which leads to the blocking of G2/M phase of the cell cycle, hence mitosis is blocked [44].

2.3.6.6 Inhibition of Notch-1 and Survival Pathways

While analyzing colon cancer cell lines (HCT-116, SW-480, SW-620), Notch-1 signaling pathway is suppressed and pro-survival molecules such as Akt, NF-$\kappa\beta$ are downregulated [26].

2.3.6.7 STAT3 Inhibition

In breast cancer cells analysis, STAT3 activity is inhibited by Withaferin-A, as a result cell migration and invasion are reduced and apoptosis is induced [26].

2.3.6.8 Caspase Activation

In HepG2 liver cancer cells analysis, activity of caspase-3, -8, and -9 is elevated, eventually leading to enhanced programmed cell death [26].

2.3.6.9 HSP90 Inhibition

HSP90 is a chaperone protein that works for the stability of cancer promoting proteins. *Withania somnifera* suppress its production, hence tumor cell survival is prohibited [45]. 10. IL-6/STAT3 inhibition (Renal cancer): In kidney cancer cell analysis, phosphorylation of STAT3 is blocked which was activated by IL-6 causing apoptosis. It triggers endoplasmic reticulum stress, which activates the transcription factor CHOP, leading to apoptotic cell death [45].

2.3.7 Therapeutic Potential of *Withania somnifera*

Figure 2.6 illustrates the therapeutic potential of *Withania somnifera* by highlighting the medicinal properties associated with different parts of the plant.

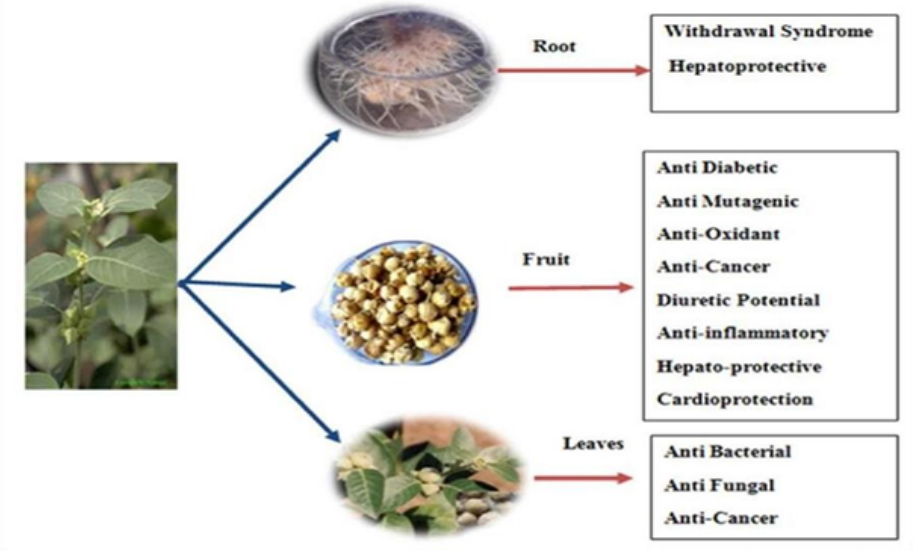

FIGURE 2.6: Phytochemistry, Food Application, Therapeutic Potential of the Plant *Withania somnifera* [24]

The roots are traditionally used for managing withdrawal symptoms and exhibit hepatoprotective effects, while the fruits demonstrate a wide range of biological activities, including antidiabetic, antioxidant, anti-mutagenic, anti-inflammatory, anticancer, diuretic, hepatoprotective, and cardioprotective properties. The leaves are particularly known for their antibacterial, antifungal, and anticancer activities. This part-specific distribution of therapeutic effects reflects the diverse phytochemical composition of *W. somnifera* and supports its extensive use in traditional medicine as well as its growing relevance in modern pharmacological research (Figure 2.6) [24].

Chapter 3

Methodology

The following methodology, as illustrated in Figure 3.1, was applied to identify potential anti-gallbladder cancer compounds from *Withania somnifera* using computational approaches.

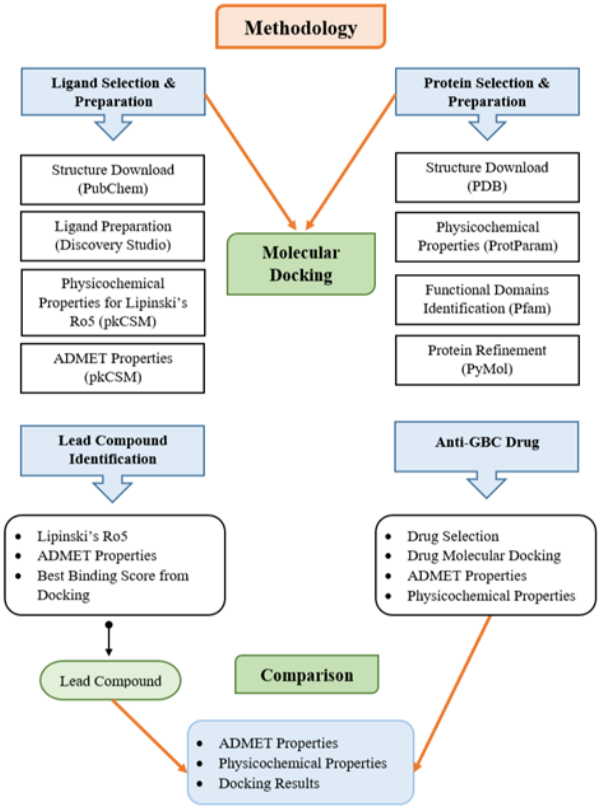

FIGURE 3.1: Methodology for the identification of the anti-GBC compound from *Withania somnifera* through computational approaches

3.1 Selection of Disease

Gallbladder cancer (GBC), known for its highly aggressive nature, late diagnosis, and limited treatment options, was selected as the target disease for this study owing to the significant impact these factors have on the poor prognosis and patient survival rates.

According to the GLOBOCAN data 2022, GBC ranks 22nd among the leading causes of cancer-related mortality worldwide. Regarding current treatment strategies, genetic analysis of GBC enlightened as with valuable information related to molecular mechanisms involved leading to the targeted therapies e.g, HER2 inhibitors (trastuzumab, pertuzumab).

However, these therapies are costly and patients in developing countries cannot afford such treatments. Moreover, their therapeutic response in advanced stages of the disease remains limited. Therefore, the development of effective, affordable, and accessible therapeutic alternatives for controlling gallbladder cancer progression remains a critical unmet need. Despite considerable research efforts, significant gaps persist in the management of this malignancy [46].

3.2 Selection and Preparation of Protein

This section outlines the process involved in the selection and preparation of the target protein for subsequent analysis.

3.2.1 Protein Selection

Initially, the target protein implicated in gallbladder cancer was selected. Due to its substantial role in the progression of malignancy, the selection of a specific protein was considered essential. The development of gallbladder cancer was significantly influenced by mutations in TP53, EGFR, and PIK3CA [47].

3.2.2 Three-Dimensional Structure

The study of protein molecular motion and conformational diversity plays a vital role in understanding of their bio-molecular mechanism and the therapeutic efficacies [48]. Three-dimensional protein structures were downloaded from the Protein Data Bank in PDB format. Protein structural data can be found in the Protein Data Bank (https://www.rcsb.org/), a major database.

3.2.3 Determination of Physiochemical Properties of Proteins

A protein's physical and chemical properties, which are essential to its stability and efficacy, define its structural and functional features. The structural and biological features of proteins can be assessed by the physicochemical properties of the proteins. It's a core component of computational analysis [49].

The physicochemical parameters of the TP53 were computed by ExPASy ProtParam. This tool is capable of calculating both pI and mW along with amino acid composition and atomic composition. In addition to these parameters, extinction coefficient was also predicted by this tool along with the estimated half-life, and instability index. The input was given in the amino acid protein sequence [50].

3.2.4 Determination of Functional Domains of Target Protein

Functional annotation is a crucial mechanism as it seeks to outline protein's identity in three different dimensions: final location, functions, and biological activities [51]. The TP53 protein's functional domains were found using the Pfam database. Protein domains were identified by Pfam (http://pfam.xfam.org/) using sequence alignments, hidden Markov models, and manual curation.

3.2.5 Refinement of Proteins

The target protein must be prepared by eliminating the naturally occurring ligand molecules that are linked to it before molecular docking can begin. This procedure makes molecular docking more effective by removing protein binding sites from ligands. PyMol software was utilized to improve the protein by eliminating water molecules, oligosaccharides, and co-crystallized ligands.

3.3 Selection and Preparation of Ligands

This section outlines the process involved in the selection and preparation of the ligands for subsequent analysis.

3.3.1 Downloading Structures of Phytochemicals

Secondary metabolites of *Withania somnifera* were chosen by reviewing the literature. A comprehensive database of chemical compound information is provided by Pub Chem. For tasks like toxicity and bioactivity prediction, virtual screening, and the identification of possible medicinal compounds, researchers use its vast amount of data. It helps with a variety of computational and experimental tasks in the fields of chemistry and drug development by making it easier to retrieve SMILES notation and three-dimensional structures in sdf format.

3.3.2 Refinement of Ligands

Downloaded ligands were subjected to energy minimization before molecular docking. This process optimizes the structure of ligands where they achieve a stable conformation with the lowest energy. This is a necessary step as the retrieved 2D structure of ligands is energetically unstable. The energy of ligand structures was minimized by the MM2 method by using the software Discovery Studio and the resulting compounds were saved in pdb.

3.4 Molecular Docking

In structure based drug design, molecular docking is the most extensively studied method. It is an approach to identify the major binding modes of a protein with a ligand. It is a key tool *in silico* drug design. The docking procedure identifies high-dimensional spaces and uses a scoring feature based on which the candidate dockings can be ranked [52]. For this purpose, the selected ligands were used against the target proteins. This process was done through Auto-Dock Vina.

3.4.1 Ligand-Protein Interaction

The interaction of ligands and the active site of the protein were analyzed to interpret docking results after obtaining the docking complex. For this purpose, PyMol was used to study hydrogen bonding and hydrophobic interactions. This tool generated a 2D representation of receptor-ligand interactions.

3.5 Virtual Screening

Virtual screening was employed to evaluate potential compounds based on their drug-likeness and pharmacokinetic properties prior to further computational analysis.

3.5.1 Lipinski's Rule of Five

It was applied to predict the pharmacological profile of selected compounds. The "Rule of Five" was used to analyze compounds during drug optimization and de signing for their good permeability and solubility likelihood. It eliminates lead compounds that have poor physicochemical properties for oral bioavailability. It is called as "Rule of Five" because the parameter values are multiples of 5. According to this rule, only compounds are selected that fulfill three or more of these physicochemical properties [53]:

i. Molecular masses $\leq$ 500 Da

ii. H-bond donors $\leq$ 5

iii. H-bond acceptors $\leq$ 10

iv. Calculated Log P (CLogP) $\leq$ 5

For the calculation of Lipinski's Ro5, the pkCSM tool was used. This tool provides information about the physicochemical properties of a given compound that was applied in Ro5.

3.5.2 ADMET Properties

A medication's absorption, distribution, metabolism, excretion, and toxicity (AD MET) were all evaluated early in the drug development process. A molecule needs to have certain characteristics in order to work as a medication. When it reaches the target place, its concentration must be sufficient, and it must remain there for a specific amount of time in order to produce the necessary biological activities and events. The pkCSM tool was utilized to assess ADMET characteristics. The method predicted physiochemical and ADMET properties after chemical smiles were added as input. pkCSM predicted the pharmacokinetic and toxicological characteristics of chemical substances using graph-based signatures. By forecasting the safety, potency, and drug-likeness of chemical compounds, this technology helped in the creation of new drugs [54].

3.6 Lead Compound

Using Lipinski's Ro5 as a primary filter and ADMET characteristics as a secondary filter, the lead compound was chosen. The docking scores and protein-ligand interaction was then analyzed. The compound chosen as a lead compound was the one with the greatest binding scores and all necessary parameters met.

3.7 Drug Selection and Screening

This section describes the identification, selection, and computational screening of potential therapeutic drugs against gallbladder cancer using database-driven approaches.

3.7.1 Anti-GBC Drug Identification

The medications that are used to treat Gallbladder cancer was identified. The KEGG disease database was used for purpose.

3.7.2 Drug Selection

To select a suitable medication, the identified drugs were filtered. The analysis was performed based on parameters such as mechanism of action, side effects, physicochemical characteristics, and ADMET properties. The physicochemical and ADMET characteristics, side effects, and mechanisms of action of the identified drugs were determined using the PubChem, pkCSM, and KEGG databases, respectively.

3.7.3 Drug Docking

The selected medication was then docked with the TP53 protein to determine and assess its modulatory potential. AutoDock Vina was used for this purpose.

3.8 Comparison with Standard Drug

The proposed anti-GBC compounds were compared with standard drug through their ADMET, physiochemical properties, and docking results.

Chapter 4

Results and Discussion

4.1 Selection and Preparation of Protein

The results related to the selection and preparation of the target protein are presented in this section.

4.1.1 3D Structure

Proteins are conformationally dynamic in nature. Their structure defines their functions, so it is essential to understand protein's structure in order to predict or assess its function. Amino acid sequence is used to generate the three-dimensional structure of protein via different software. The accuracy in structural prediction is achieved via advancement in the computational algorithms and tools [55].

Protein Data Bank (PDB) was used to download the 3D structure of TP53 with PDB ID of 9EWW as shown in the Figure 4.1. The structure was determined using electron microscopy with a reported resolution of 8.57 $\mathring{A}$. The protein was analyzed in a particle aggregation state, and the 3D model was generated through a single-particle reconstruction method. The total structural weight was 38.39 kDa.

FIGURE 4.1: 3D Structure of the TP53 Protein

4.1.2 Physiochemical Properties

The physicochemical properties of proteins are critically important in the context of therapeutic development and biological function because they directly influence numerous key aspects of protein behavior, stability, and interactions within biological systems [56].

i. Protein Stability and Folding: Physicochemical properties such as hydrophobicity, charge distribution, and hydrogen bonding influence how a protein folds into its functional three-dimensional structure. Proper folding is essential for maintaining biological activity, while misfolding can lead to aggregation or degradation. Understanding these properties helps in designing stable protein formulations that retain activity over time [56].

ii. Solubility and Aggregation: Aqueous solubility is vital for proteins to function effectively in vivo and during manufacturing processes. Proteins with

poor solubility are prone to aggregation, which can reduce efficacy and increase immunogenicity. Controlling properties like surface hydrophobicity and charge can improve solubility and reduce unwanted aggregation [56].

iii. Pharmacokinetics and Bio-distribution: Physicochemical traits such as size, charge, and hydrophobicity affect how proteins distribute in the body, their half-life, and tissue penetration. For example, highly hydrophobic proteins may nonspecifically bind to cell membranes or serum components, altering their pharmacokinetic profile [56].

iv. Manufacturability and Formulation: Optimal physicochemical properties facilitate large-scale manufacturing and formulation development. Stable, soluble proteins are easier to purify, store, and deliver via injection or other routes. Variations in properties like surface charge and hydrophobicity influence formulation stability and shelf-life [56].

v. Immunogenicity: Altered or abnormal physicochemical properties can increase the risk of immunogenic responses. For instance, exposed hydrophobic patches or aggregates can be recognized by the immune system, potentially leading to adverse reactions [56].

vi. Interaction with Target and Off-Target Molecules: Hydrogen bonding capabilities, charge, and hydrophobic regions determine the binding affinity and specificity of proteins to their targets. These properties influence therapeutic efficacy, as well as potential off-target effects [56].

ProtParam ExPASy was used to calculate physiochemical properties. The input was given by using amino acid sequence of TP53 protein. The instability index, at 65.27, indicates the protein's instability with an index greater than 40. The protein's hypothetical pI (pH 4.62) indicates that it is in acidic form. The protein is 213574.41Dalton in the molecular weight, 67.67in the aliphatic index, and -0.700 in the GRAVY, respectively. If a protein has an instability index above 40, it is considered unstable; if it is below 40, it is deemed stable [57]. The isoelectric point (pI) of a protein is defined as the pH at which the net charge

of a protein molecule is zero. Accordingly, proteins are positively charged at a pH below their pI and negatively charged at a pH above their pI. The protein pI varies greatly from extremely acidic to highly alkaline values ranging from about 4.0 to 12.0 [58]. GRAVY (Grand Average of Hydropathy) refers to the average hydropathy values of the amino acids in a protein [59]. An amino acid sidechain's hydrophilic and hydrophobic properties are indicated by a value in the hydropathy index. Hydrophobic proteins are those with a positive GRAVY. The hydrophobicity increases as the number increases. Low GRAVY indicates better interaction with water molecules. Finding the protein GRAVY is essential for protein-ligand interaction in solution [60]. The measurement of a protein's light absorption in water at 280 nm yields its extinction coefficient, sometimes referred to as molar absorptivity. This coefficient is influenced by the concentrations of tyrosine (Tyr), tryptophan (Trp), and cystine (a disulphide). Two values are calculated by ProtParam: one that accounts for each Cys residue from cystines and another that accounts for each Cys residue that is reduced. Half-life calculates the amount of time it will take for half of a cell's protein synthesis to cease. ProtParam predicts a protein's half-life by analysing its N-terminal amino acids [59]. The physicochemical properties of the TP53 protein, as predicted using the ExPASy ProtParam tool, are summarized in Table 4.1.

4.1.3 Functional Domains

Most proteins in cells are composed of multiple folding units (or domains) to perform complex functions in a cooperative manner [61]. The protein's functional domains as predicted by the pfam tool can be shown in Figure 4.2.

4.1.4 Refinement of the Protein

Pre-docking protein preparation was done by removing ligands, hetatoms and water molecules with pyMol software. Figure 4.3 shows the refined 3D structure of TP53 Protein.

TABLE 4.1: Physicochemical properties of TP53 (ProtParam).

Sr. no.	**Properties**	**Results**
1	Number of amino acids	1972
2	Theoretical pI	4.62
3	Molecular weight	213574.41
4	Total number of negatively charged residues (Asp + Glu)	330
5	Total number of positively charged residues (Arg + Lys)	182
6	Total number of atoms	29523
7	Extinction coefficient (with all cys residues)	86480
8	Extinction coefficient (all cys residues reduced)	84230
9	Estimated half-life	>30 hours (mammalian reticulocytes, in vitro) >20 hours (yeast, in vivo) >10 hours (*Escherichia coli*, in vivo)
10	Instability index	65.27
11	Aliphatic index	67.67
12	Grand average of hydropathicity (GRAVY)	-0.700
13	Formula	$C_{9129}H_{14565}N_{2563}O_{3198}S_{68}$
14	Atomic composition	Carbon (C): 9129 Hydrogen (H): 14565 Nitrogen (N): 2563 Oxygen (O): 3198 Sulfur (S): 68

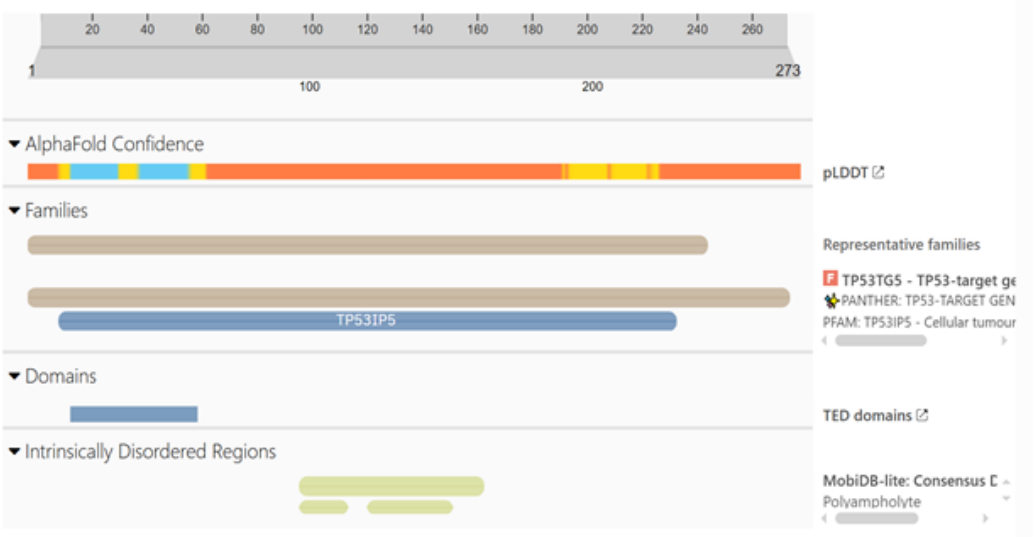

FIGURE 4.2: AlphaFold-based annotation of TP53 illustrating pLDDT confidence scores, predicted domains, intrinsically disordered regions, and conserved functional residues relevant to protein-protein and ligand interactions. (Pfam)

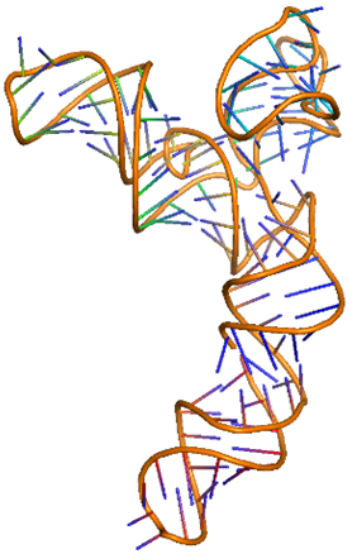

FIGURE 4.3: Refined 3D Structure of TP53 Protein (PyMol)

4.2 Selection and Preparation of Ligand

The results related to the selection and preparation of the ligands are presented in this section.

4.2.1 Ligand Physicochemical Properties and Structure

The table 4.2 shows 3D structures and information of selected ligands downloaded from PubChem.

4.2.2 Ligand Refinement

The energy minimization method was used to prepare the pre-docking ligand. Through this method, ligands' structures are optimized to get the lowest energy and most stable conformation. Due to the energetic instability of the ligands' recovered 2D structure, this step is essential.

TABLE 4.2: Physicochemical properties and structure of ligands (PubChem).

Sr. no.	Ligand	PubChem CID	Formula	Mol. wt	Structure
1	Withaferin A	265237	$C_{28}H_{38}O_6$	470.6 g/mol	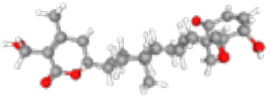
2	Withanolide D	161671	$C_{28}H_{38}O_6$	470.6 g/mol	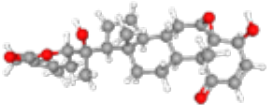
3	Withanone	21679027	$C_{28}H_{38}O_6$	470.6 g/mol	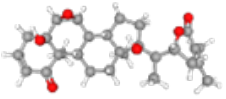
4	Withanolide A	11294368	$C_{28}H_{38}O_6$	470.6 g/mol	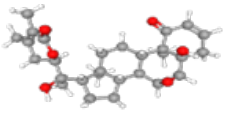
5	Withanolide E	301751	$C_{28}H_{38}O_7$	486.6 g/mol	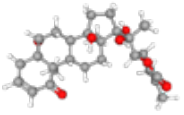
6	Withanolide F	135887	$C_{28}H_{40}O_7$	488.6 g/mol	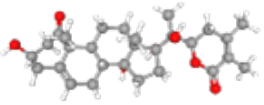

4.3 Molecular Docking

Molecular docking is a technique that is used for the estimation of the strength between a ligand bonded to a receptor protein through the vina score function and for determining the correct structure of the ligand that binds to the binding site [62]. Molecular docking was performed to investigate the potential binding interaction between the tumor suppressor protein TP53 and the phytochemical Withaferin A, a bioactive constituent of *Withania somnifera*. AutoDock Vina was employed as the scoring function, with the receptor treated as rigid and the ligand as flexible. The docking grid was centered to encompass the predicted binding region of TP53.

4.3.1 Docking Parameters

i. Protein (Receptor): TP53

ii. Ligand: Six different ligands

iii. Scoring function: AutoDock Vina

iv. Grid center: X = 90.428, Y = 89.999, Z = 88.821

v. Grid size: 26 × 26 × 26 Å

vi. Grid spacing: 1 Å

vii. Exhaustiveness: 8

These parameters are within acceptable limits for reliable docking and ensure adequate sampling of ligand conformations within the selected region.

4.3.2 Docking Interaction Analysis of Withaferin A against TP53

The docking result of TP53 and Withaferin A generated nine binding modes as shown in Table 4.3 The best-ranked pose (Mode 1) exhibited the following characteristics:

i. Binding affinity: −7.669 kcal/mol

ii. RMSD (lower and upper bound): 0.0 Å (reference pose)

A binding affinity of -7.669 $kcal/mol$ indicates a favorable and thermodynamically stable interaction between Withaferin A and TP53. In molecular docking studies, binding energies in the range of -6.0 to -8.0 $kcal/mol$ are generally considered biologically meaningful, suggesting a reasonable likelihood of interaction under physiological conditions. The remaining poses showed slightly higher (less negative) binding energies ranging from -7.495 to -7.23 kcal/mol, indicating consistent binding behavior across multiple conformations. The RMSD values relative to the best mode ranged from approximately 1.27 $\mathring{A}$ to > 10 $\mathring{A}$, suggesting the presence of both closely related and distinctly different binding orientations. The presence of

TABLE 4.3: Docking Result of Withaferin A with TP53

Mode	Binding Affinity (kcal/mol)	Distance from Best Mode	
		RMSD l.b. (Å)	**RMSD u.b. (Å)**
1	-7.669	0.000	0.000
2	-7.495	9.087	13.430
3	-7.440	1.269	1.361
4	-7.359	7.640	15.770
5	-7.330	7.170	11.560
6	-7.301	9.020	16.730
7	-7.299	10.920	14.550
8	-7.230	3.417	5.036
9	-7.230	2.936	5.391

low-RMSD, low-energy poses suggests that Withaferin A repeatedly binds to the same general region of TP53, reinforcing the reliability of the predicted binding site.

Previous studies have demonstrated that Withaferin A activates wild-type p53 and disrupts mortalin-p53 interactions, leading to p53 nuclear translocation and reactivation in cancer cells. Bioinformatics and experimental analyses further support its selective binding to mutant p53 variants, highlighting its potential as a p53-modulating anticancer agent. These findings corroborate the stable interaction observed in the present docking analysis of Withaferin A with TP53 [63].

4.3.3 Docking Interaction Analysis of Withanolide A against TP53

The docking simulation of TP53 and Withanolide A generated seven binding modes, as shown in Table 4.4, with the best-ranked pose exhibiting a binding affinity of -8.583 kcal/mol (Mode 1).

This binding energy indicates a strong and favorable interaction between TP53 and Withanolide A. Compared to typical docking benchmarks, values below -8.0 kcal/mol are considered indicative of high binding stability. The remaining docking modes displayed binding affinities ranging from -8.461 to -8.183 kcal/mol,

TABLE 4.4: Docking result of Withanolide A with TP53

Mode	Binding Affinity (kcal/mol)	Distance from Best Mode	
		RMSD l.b. ($\AA$)	**RMSD u.b.** ($\AA$)
1	-8.583	0.000	0.000
2	-8.461	5.458	11.650
3	-8.374	8.016	14.550
4	-8.339	4.055	7.711
5	-8.311	4.069	7.642
6	-8.265	2.618	3.957
7	-8.183	8.569	13.880
8	-8.583	0.000	0.000
9	-8.461	5.458	11.650

demonstrating a narrow energy distribution. This clustering of energy values suggests reproducible binding behavior and reinforces the reliability of the predicted interaction. Mode 1 exhibited an RMSD value of 0.0 $\AA$ and was therefore considered the reference pose. Modes 5 and 6 showed RMSD values in the range of approximately 2-4 $\AA$, indicating structurally similar and energetically comparable binding conformations. In contrast, modes with higher RMSD values (>5 $\AA$) represented alternative and less favorable ligand orientations within the binding site. Overall, the presence of low-energy docking poses with acceptable RMSD values supports the stability and reliability of the predicted binding mode.

Previous experimental studies have shown that Withanolide A interacts selectively with mutant p53, particularly the p53ˆY220C variant, inducing conformational stabilization and restoration of wild-type tumor suppressor activity. These findings support its ability to bind p53 and modulate its structure, consistent with the stable surface-binding interaction observed in the present TP53 docking analysis [63].

4.3.4 Docking Interaction Analysis of Withanolide E against TP53

The docking result of TP53 and Withanolide E produced nine binding modes, as shown in Table 4.5, with the best-ranked pose exhibiting a binding affinity of

-8.316 kcal/mol (Mode 1). This value indicates a strong and favorable interaction between TP53 and Withanolide E. Binding energies below -8.0 kcal/mol are gener-

TABLE 4.5: Docking result of Withanolide E with TP53 protein

Mode	**Binding Affinity (kcal/mol)**	**Distance from Best Mode**	
		RMSD l.b. ($\AA$)	**RMSD u.b.** ($\AA$)
1	-8.316	0.000	0.000
2	-8.069	2.382	8.884
3	-7.773	7.593	13.080
4	-7.571	5.950	9.424
5	-7.500	2.551	9.395
6	-7.454	4.432	10.590
7	-7.384	2.465	3.579
8	-7.354	3.521	5.540
9	-7.334	2.419	4.526

ally considered to reflect high binding stability in docking studies. The remaining binding modes displayed binding affinities ranging from -8.069 to -7.334 kcal/mol. The relatively narrow range of energies suggests consistent ligand binding behavior and reinforces the reliability of the docking predictions. Mode 1 exhibited an RMSD value of 0.0 $\AA$ and was therefore considered the reference pose. Modes 2, 7, and 9 showed RMSD values in the range of approximately 2-3 $\AA$, indicating structurally similar and consistent binding orientations.

In contrast, docking modes with higher RMSD values (>5 $\AA$) represented alternative and less favorable conformations. Overall, the presence of multiple low-energy poses with acceptable RMSD values supports the stability and reproducibility of the predicted binding mode. Previous molecular docking studies against the TP53 (5TRF) target protein reported a strong binding affinity for Withanolide E (-9.4 kcal/mol), demonstrating stable hydrogen bond interactions with key residues such as VAL93. These findings support the strong and favorable binding observed in the present TP53 docking analysis, reinforcing the potential of Withanolide E as a bioactive anticancer compound with significant protein interaction capability [64].

4.3.5 Docking Interaction Analysis of Withanolide F against TP53

The docking result of TP53 and Withanolide F generated nine binding modes, as shown in Table 4.6, with the best-ranked pose exhibiting a binding affinity of -9.265 kcal/mol (Mode 1). This binding energy represents a very strong interaction,

TABLE 4.6: Docking result of Withanolide F with TP53 protein

Mode	**Binding Affinity (kcal/mol)**	**Distance from Best Mode**	
		RMSD l.b. (*Å*)	**RMSD u.b.** (*Å*)
1	-9.265	0.000	0.000
2	-9.155	7.264	13.300
3	-8.612	4.123	9.200
4	-8.580	5.740	8.925
5	-8.357	2.007	3.356
6	-8.265	2.559	9.322
7	-7.829	2.366	9.231
8	-7.724	6.103	9.301
9	-7.716	9.659	13.830

surpassing the affinities observed for all previously analyzed withanolides. Binding energies below -9.0 kcal/mol are generally indicative of high binding strength and strong thermodynamic favorability in molecular docking studies. The second-ranked pose also displayed a very strong affinity (-9.155 kcal/mol), while several additional modes showed energies between -8.6 and -8.3 kcal/mol. This clustering of low-energy poses indicates robust and reproducible binding behavior. Mode 1 displayed an RMSD value of 0.0 $\mathring{A}$ and was therefore considered the reference binding pose. Modes 5 and 6 showed RMSD values in the range of approximately 2-3 $\mathring{A}$, indicating structurally similar and reliable binding conformations. In contrast, docking modes with higher RMSD values (>5 $\mathring{A}$) represented alternative and less favorable orientations. Overall, the presence of multiple low-energy poses with acceptable RMSD values further supports the stability of the predicted binding mode.

4.3.6 Docking Interaction Analysis of Withanolide D against TP53

The docking generated nine binding modes, as shown in Table 4.7, with the best-ranked pose showing a binding affinity of -8.534 kcal/mol (Mode 1). This value indicates a strong and favorable interaction between TP53 and Withanolide D. Binding energies in the range of -8.0 to -9.0 kcal/mol are generally considered

TABLE 4.7: Docking result of Withanolide D with TP53 protein

Mode	**Binding Affinity (kcal/mol)**	**Distance from Best Mode**	
		RMSD l.b. ($\AA$)	**RMSD u.b.** ($\AA$)
1	-8.534	0.000	0.000
2	-8.251	4.372	8.655
3	-8.209	6.959	11.460
4	-8.154	6.409	10.860
5	-8.116	4.303	8.334
6	-8.101	4.575	7.396
7	-8.083	2.205	3.848
8	-8.027	2.700	8.504
9	-8.006	5.906	9.133

indicative of stable protein-ligand interactions in molecular docking studies. The remaining docking modes exhibited binding affinities ranging from -8.251 to -8.006 kcal/mol, reflecting a narrow distribution of energy values. This consistency suggests reproducible binding behavior and reinforces the reliability of the docking predictions. Mode 1 exhibited an RMSD value of 0.0 $\AA$ and was therefore considered the reference binding pose. Modes 7 and 8 showed RMSD values of approximately 2-3 $\AA$, indicating structurally similar binding orientations. In contrast, docking modes with higher RMSD values (>4 $\AA$) represented alternative and less favorable conformations. Overall, the presence of low-energy poses with acceptable RMSD values supports the stability of the predicted binding mode.

Withanolide D exhibited one of the highest binding affinities in prior docking studies (-10.1 kcal/mol) against the 5TRF protein, forming stable hydrogen bonds with critical residues including VAL93 and HIS96. This strong binding profile aligns

with the favorable docking interactions observed in the current TP53 analysis, supporting its potential role as a biologically active anticancer agent [64].

4.3.7 Docking Interaction Analysis of Withanone against TP53

The docking produced nine binding modes, as shown in Table 4.8, with the best-ranked pose exhibiting a binding affinity of -8.704 kcal/mol (Mode 1). This binding energy indicates a strong and favorable interaction between TP53 and Withanone.

TABLE 4.8: Docking results of Withanone with TP53 protein

Mode	**Binding Affinity (kcal/mol)**	**Distance from Best Mode**	
		RMSD l.b. ($\AA$)	**RMSD u.b.** ($\AA$)
1	-8.704	0.000	0.000
2	-8.643	4.699	8.855
3	-8.541	9.827	14.950
4	-8.398	1.925	9.217
5	-8.282	4.712	8.691
6	-8.270	1.784	9.131
7	-8.238	2.783	9.624
8	-8.079	2.997	9.852
9	-3.844	10.550	15.720

Binding affinities below -8.0 kcal/mol are generally considered indicative of stable and biologically meaningful protein-ligand interactions. The remaining docking modes displayed binding affinities ranging from -8.643 to -8.079 kcal/mol, with one low-ranking outlier (-3.844 kcal/mol). The clustering of most binding energies within a narrow range indicates consistent and reproducible binding behavior.

Mode 1 exhibited an RMSD value of 0.0 $\AA$ and was therefore considered the reference binding pose. Modes 4, 6, and 7 showed RMSD values in the range of approximately 1.7-2.8 $\AA$, indicating structurally similar and reliable binding conformations. In contrast, docking modes with higher RMSD values (>4 $\AA$) represented alternative and less favorable orientations. Overall, the presence of

multiple low-energy poses with acceptable RMSD values supports the stability of the predicted binding mode.

Earlier docking analyses reported that Withanone demonstrated a notable binding affinity (-8.9 kcal/mol) with stable hydrogen bonding interactions involving key residues such as GLY58. These results validate the present docking findings, where Withanone also showed stable surface binding with TP53, indicating its potential as a regulatory modulator in cancer-related protein interactions [64].

4.3.8 Comparative Docking Analysis of Selected Compounds with TP53

Table 4.9 presents a comparative analysis of the docking results of selected *Withania somnifera* derived phytochemicals against the target protein i.e. TP53.

TABLE 4.9: Comparative analysis of the docking results.

Sr. no.	**Ligand**	**Best binding affinity (kcal/mol)**	**Interaction strength**
1	Withaferin A	−7.669	Moderate
2	Withanolide E	−8.316	Strong
3	Withanolide D	−8.534	Strong
4	Withanolide A	−8.583	Strong
5	Withanone	−8.704	Strong-Very strong
6	Withanolide F	−9.265	Very strong

Among the evaluated ligands, Withaferin A showed the weakest interaction with a binding affinity of −7.669 kcal/mol, corresponding to moderate interaction strength.

In contrast, Withanolide E, Withanolide D, and Withanolide A exhibited stronger binding affinities ranging from −8.316 to −8.583 kcal/mol, indicating strong interactions with the target protein. Withanone demonstrated an enhanced interaction profile with a binding affinity of −8.704 kcal/mol, categorized as strong to very strong.

Notably, Withanolide F displayed the highest binding affinity (−9.265 kcal/mol), reflecting a very strong interaction and suggesting superior binding stability compared to the other compounds. Overall, the docking results summarized in Table 4.9 highlight Withanolide F as the most promising candidate for effective modulation of the target protein.

4.4 Ligand-Protein Interaction

Interactions of ligands and target proteins were analyzed through Pymol that generates 2D structures from 3D coordinates.

4.4.1 Molecular Interaction Analysis of Withaferin A with TP53 Protein

The molecular docking analysis indicates that Withaferin A binds to a surface-accessible region of the TP53 protein rather than a deeply buried pocket, as shown in figure 4.4. The ligand adopts a stable orientation along a shallow surface groove, consistent with the regulatory nature of TP53, whose activity is primarily governed by conformational changes and protein-protein interactions.

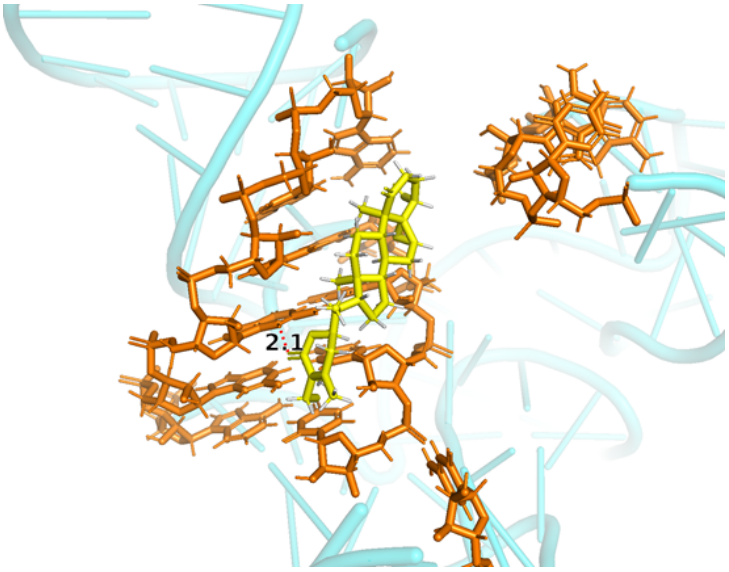

FIGURE 4.4: Interaction of Withaferin A with Receptor Protein

The interaction is stabilized by a combination of hydrogen bonding and hydrophobic contacts. A hydrogen bond with an approximate distance of 2.1 $\mathring{A}$ is observed between Withaferin A and a nearby TP53 residue, indicating a strong non-covalent interaction. In addition, the steroidal scaffold of Withaferin A engages surrounding hydrophobic residues, contributing to ligand stabilization through van der Waals and hydrophobic interactions. Residues located within close proximity ($\leq$6 $\mathring{A}$) of the ligand collectively anchor Withaferin A on the protein surface, suggesting cooperative stabilization rather than reliance on a single interaction. Overall, this binding mode suggests that Withaferin A may function as a potential allosteric modulator of TP53, supporting its proposed anticancer role through indirect modulation of TP53 activity rather than direct active-site inhibition. This *in silico* evidence supports previously reported experimental findings demonstrating the anticancer potential of Withaferin A across multiple cancer types, including breast cancer, where it has been shown to modulate TP53-related pathways, induce apoptosis, and inhibit tumor cell proliferation [65].

4.4.2 Molecular Interaction Analysis of Withanolide A with TP53 Protein

The interaction, as shown in figure 4.5, of Withanolide A with target protein shows that ligand bound to a surface-accessible region of TP53, where nearby amino acid residues form stabilizing interactions. The ligand adopts a compact orientation that aligns its steroidal scaffold along the protein surface, indicating a non-catalytic, regulatory binding mode.

Multiple hydrogen bonds are observed between Withanolide A and TP53, with bond distances ranging from 1.9 to 2.8 $\mathring{A}$, reflecting strong and favorable non-covalent interactions. These interactions are complemented by hydrophobic and van der Waals contacts with surrounding residues, which further stabilize the complex. Overall, the interaction pattern suggests that Withanolide A may act as a potential allosteric modulator of TP53, with the observed hydrogen bond network and favorable binding geometry supporting its strong docking affinity. Previous

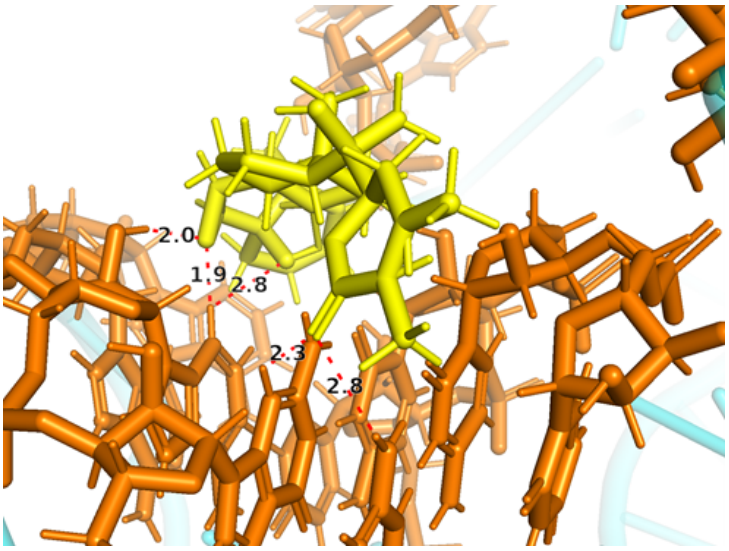

FIGURE 4.5: Interaction of Withanolide A with Receptor Protein

experimental studies have shown that Withanolide A exhibits significant antiproliferative and pro-apoptotic activity in breast cancer models, where it effectively inhibits cancer cell growth and induces apoptosis through modulation of key regulatory pathways, including p53 signaling [65].

4.4.3 Molecular Interaction Analysis of Withanolide E with TP53 Protein

As shown in Figure 4.6, the docking pose illustrates Withanolide E (yellow) bound to a surface-exposed region of TP53, which is consistent with the regulatory nature of the protein, whose function is primarily mediated through conformational changes and protein-protein interactions rather than through a deeply buried catalytic active site. The ligand interacts closely with surrounding TP53 residues (orange), forming a stable interaction environment.

A hydrogen bond with an intermolecular distance of approximately 2.4 $\mathring{A}$ is observed, indicating a strong and favorable polar interaction that contributes to complex stabilization. Additionally, the steroidal framework of Withanolide E establishes hydrophobic and van der Waals interactions with nearby residues, further enhancing binding affinity. Overall, these interactions suggest that Withanolide E

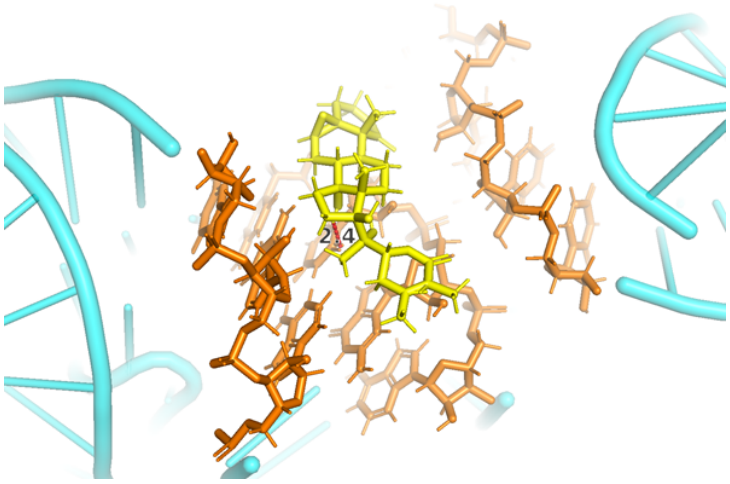

FIGURE 4.6: Interaction of Withanolide E with Receptor Protein

may function as a potential allosteric modulator of TP53, with favorable binding geometry and interaction stability supporting its docking performance. These observation aligns well with experimental evidence reported in the literature, where Withanolide E has demonstrated significant anticancer activity through modulation of apoptosis-related signaling pathways. Previous studies have shown that Withanolide E sensitizes cancer cells to apoptosis by promoting degradation of cFLIP and selectively modulating HSP90 client proteins, thereby enhancing death receptor-mediated apoptotic signaling while exhibiting minimal toxicity as a single agent [66].

4.4.4 Molecular Interaction Analysis of Withanolide F with TP53 Protein

The docking visualization presented in Figure 4.7 demonstrates that Withanolide F (yellow) interacts favorably with TP53 at a surface-accessible binding region, supporting the regulatory and allosteric nature of TP53. This binding mode suggests a potential role in modulating TP53 conformation rather than occupying a deeply buried pocket.

Multiple hydrogen bond interactions are observed between Withanolide F and surrounding TP53 residues (orange), with bond distances ranging from 2.2 to 2.7

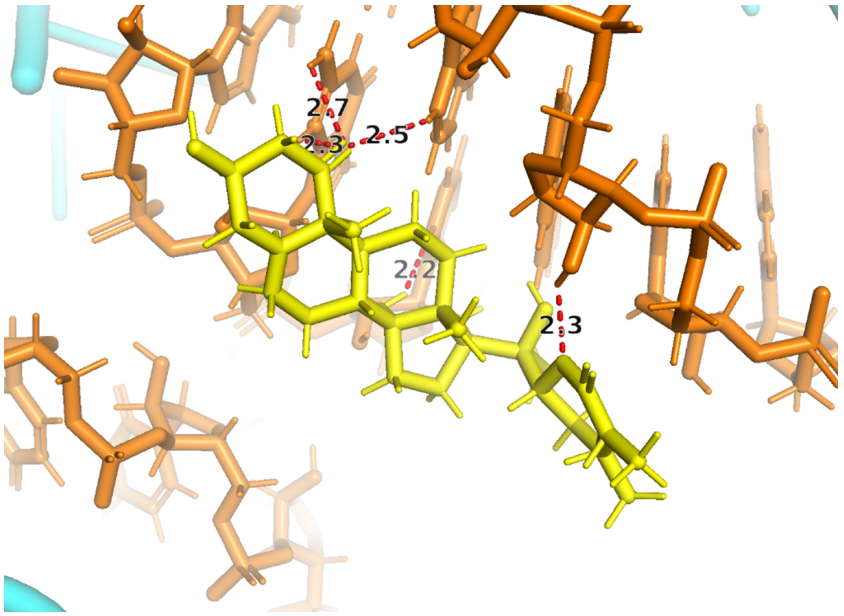

FIGURE 4.7: Interaction of Withanolide F with Receptor Protein

Å, indicating strong and energetically favorable interactions. The presence of multiple hydrogen bonds suggests cooperative stabilization of the ligand-protein complex.

In addition, the steroidal backbone of Withanolide F forms extensive hydrophobic and van der Waals interactions with adjacent amino acid residues, further enhancing binding stability and maintaining a favorable ligand orientation.

Overall, these interactions indicate that Withanolide F exhibits strong and stable binding affinity toward TP53 and may act as a potential allosteric modulator. Among the tested compounds, the multiple short hydrogen bond distances highlight Withanolide F as a particularly promising TP53-interacting phytochemical.

Withanolide F has demonstrated notable in vitro anticancer activity, particularly by inhibiting cancer cell proliferation and suppressing NF-$\kappa\beta$ signaling, a pathway closely associated with TP53 regulation. Previous studies have reported its low micromolar antiproliferative effects against multiple myeloma cancer stem cells and RPMI-8226 cells. Consistent with these findings, the surface-accessible and non-catalytic binding of Withanolide F to TP53 observed in this study supports its role as a regulatory modulator [67].

4.4.5 Molecular Interaction Analysis of Withanolide D with TP53 Protein

Withanolide D binds to a surface-exposed region of TP53, as shown in Figure 4.8, consistent with the allosteric binding behavior commonly observed for TP53-small molecule interactions. The ligand establishes multiple hydrogen bonds with nearby TP53 residues, with bond distances ranging from 2.4 to 2.6 $\mathring{A}$, indicating strong and favorable polar interactions. Additionally, the steroidal backbone

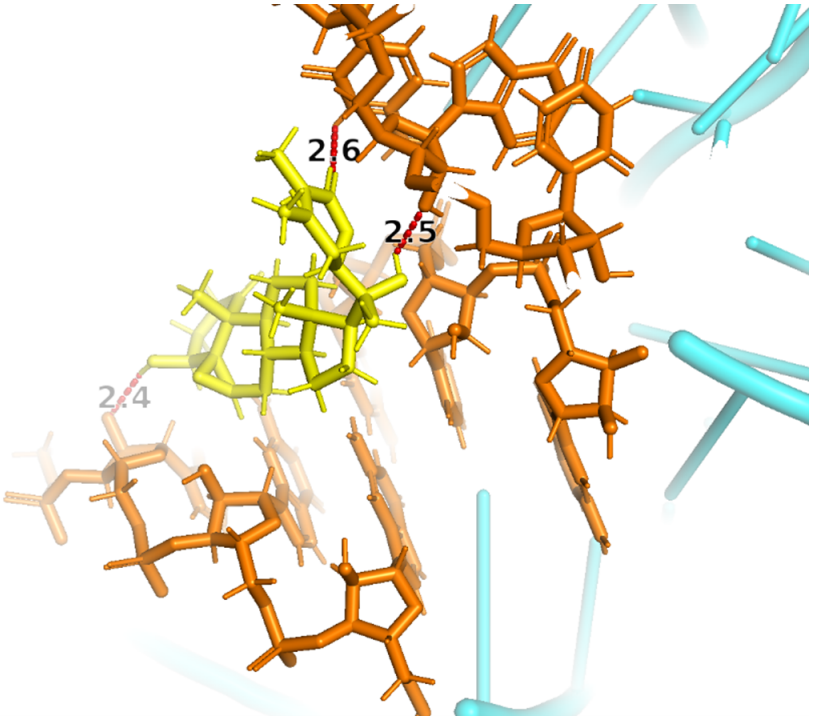

FIGURE 4.8: Interaction of Withanolide D and TP53

of Withanolide D engages in hydrophobic and van der Waals interactions with surrounding residues, which further stabilize the ligand-protein complex. The combined presence of polar and non-polar contacts suggests a stable binding conformation. Overall, Withanolide D demonstrates favorable interaction with TP53, supporting its potential role as an allosteric modulator of TP53 activity. Withanolide D has been reported to exhibit strong anticancer activity by enhancing radiosensitivity and impairing DNA damage repair mechanisms in human cancer cells. Notably, Lacombe et al. demonstrated that Withanolide D inhibits key DNA repair proteins, leading to persistent DNA damage and mitotic catastrophe,

even in p53-deficient cancer models, highlighting its role as a regulatory modulator rather than a classical cytotoxic agent [67].

4.4.6 Molecular Interaction Analysis of Withanone with TP53 Protein

The molecular docking analysis presented in Figure 4.9 shows that Withanone binds to a surface-accessible region of the TP53 protein, consistent with a non-catalytic and regulatory mode of interaction. The ligand is positioned along the protein surface, allowing its rigid steroidal framework to establish stable contacts with nearby amino acid residues.

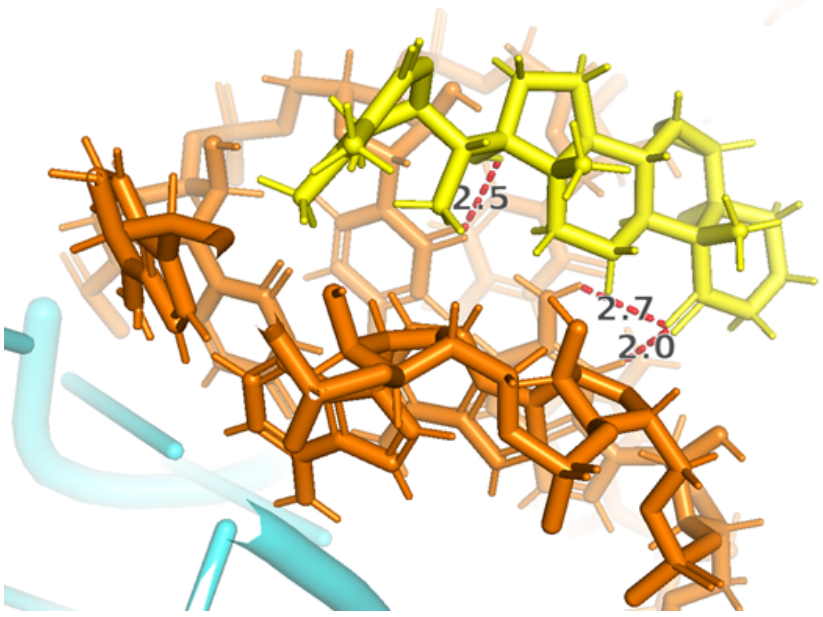

FIGURE 4.9: Interaction of Withanone with Receptor Protein

Multiple hydrogen bond interactions are observed between Withanone and TP53, with bond distances ranging approximately from 2.0 to 2.7 $\mathring{A}$, indicating strong and favorable non-covalent interactions. These hydrogen bonds contribute significantly to the stabilization of the ligand-protein complex. In addition to hydrogen bonding, Withanone engages in hydrophobic and van der Waals interactions with surrounding TP53 residues, which further enhance binding stability and maintain an optimal ligand orientation. Residues within close proximity collectively contribute to ligand anchoring, suggesting cooperative stabilization.

Overall, the interaction pattern suggests that Withanone may act as a potential allosteric modulator of TP53, potentially influencing protein conformation or regulatory interactions. The observed hydrogen bond network and favorable interaction geometry support the docking affinity of Withanone toward TP53.

The anticancer relevance of Withanone is supported by existing literature demonstrating its inhibitory effects across multiple cancer types, including breast carcinoma, glioblastoma, and neuroblastoma. Recent studies have shown that Withanone suppresses cancer cell stemness, epithelial-mesenchymal transition, and proliferation through modulation of key signaling pathways such as NF-$\kappa\beta$, PI3K/Akt, and p53, while promoting differentiation rather than inducing nonspecific cytotoxicity [68].

4.5 Drug-Likeness Evaluation Based on Lipinski's Rule of Five

Lipinski's Rule of Five (RO5) serves as a fundamental guideline in drug discovery; however, the manual evaluation of a large number of compounds is both time-consuming and resource-intensive. Lipinski's Rule of Five is particularly valuable for identifying compounds with favorable oral bioavailability and membrane permeability.

Molecules that meet these criteria are more likely to effectively interact with protein targets, thereby enhancing their potential as viable drug candidates. According to the rule, an orally active compound should typically exhibit no more than one violation of the following parameters: a molecular weight exceeding 500 Da, a calculated logP (ClogP) greater than 5, more than five hydrogen bond donors, or more than ten hydrogen bond acceptors (primarily nitrogen and oxygen atoms) [69].

As summarized in Table 4.10, the drug-likeness of selected phyto-compounds from *Withania somnifera* was evaluated using pkCSM based on Lipinski's Rule of Five.

TABLE 4.10: Lipinski's rule of five assessment of selected ligands (PkCSM).

Sr.	Ligand	MW	LogP	HBD	HBA	RB
1	Withaferin A	470.606	3.3529	2	6	3
2	Withanone	470.606	3.4954	2	6	2
3	Withanolide A	470.606	3.4954	2	6	2
4	Withanolide D	470.606	3.4954	2	6	2
5	Withanolide E	486.605	2.7544	3	7	2
6	Withanolide F	470.606	3.5432	3	6	2

Based on pkCSM predictions, all evaluated compounds fully comply with Lipinski's Rule of Five, exhibiting zero violations of the criteria. This suggests that Withaferin A, Withanone, and the assessed withanolides possess favorable physicochemical properties and are potentially suitable for oral drug development.

4.5.1 Molecular Weight Analysis

All analyzed compounds, Withaferin A, Withanone, Withanolide A, D, E, and F, exhibited molecular weights ranging from 470.6 to 486.6 Da, which fall below the 500 Da threshold recommended by Lipinski's criteria. This indicates that all compounds possess an appropriate molecular size conducive to oral absorption.

4.5.2 Lipophilicity Analysis

The predicted log P values ranged from 2.75 to 3.54, remaining well within the acceptable limit of ≤ 5. These moderate lipophilicity values suggest a balanced hydrophilic-lipophilic profile, favoring both membrane permeability and solubility.

4.5.3 Hydrogen Bond Donors Analysis

All compounds displayed 2-3 hydrogen bond donors, which is within the acceptable limit of ≤ 5. This supports efficient hydrogen bonding interactions with biological targets while maintaining favorable permeability characteristics.

4.5.4 Hydrogen Bond Acceptors Analysis

The number of hydrogen bond acceptors ranged from 6 to 7, staying below the maximum recommended value of ≤ 10. This indicates suitable polarity for interaction with protein binding sites without compromising membrane transport.

4.5.5 Rotatable Bonds Analysis

The compounds showed 2-3 rotatable bonds, reflecting low molecular flexibility. Reduced flexibility is often associated with improved binding specificity and oral bioavailability, as excessively flexible molecules may suffer from entropic penalties during target binding.

4.6 ADMET Profiling of the Selected Ligands

Drug discovery is a complex process that increasingly relies on rational, target-oriented strategies supported by modern scientific tools. In this context, the evaluation of ADMET properties, absorption, distribution, metabolism, excretion, and toxicity, is essential for predicting the pharmacokinetic behavior and safety of potential drug candidates [70].

4.6.1 Absorption Analysis

The absorption-related ADMET properties of Withaferin A, Withanone, and Withanolides A, D, E, and F were predicted using the pkCSM server, and the results are summarized in Tables 4.11 and 4.12.

All six ligands exhibited low predicted aqueous solubility, with water solubility values ranging from -5.06 to -5.25 log mol/L, indicating poor solubility in water. This behavior is typical of steroidal lactones and other hydrophobic natural

TABLE 4.11: Adsorption properties of the ligands (Withaferin A, Withanone, and Withanolide A).

Sr. no.	**Characteristic**	**Withaferin A**	**Withanone**	**Withanolide A**
1	Water solubility (log mol/L)	−5.063	−5.127	−5.096
2	Caco2 permeability (log Papp in 10^{-6} cm/s)	0.829	0.849	0.846
3	Intestinal absorption (human) (%)	85.345	100	100
4	Skin permeability (log Kp)	−3.202	−3.365	−3.285
5	P-glycoprotein substrate	Yes	Yes	Yes
6	P-glycoprotein I inhibitor	Yes	Yes	Yes
7	P-glycoprotein II inhibitor	Yes	Yes	Yes

TABLE 4.12: Adsorption properties of the ligands (Withanolide D, Withanolide E, and Withanolide F).

Sr. no.	**Characteristic**	**Withanolide D**	**Withanolide E**	**Withanolide F**
1	Water solubility (log mol/L)	−5.127	−5.252	−5.209
2	Caco2 permeability (log Papp in 10^{-6} cm/s)	0.831	0.742	−5.209
3	Intestinal absorption (human) (%)	99.2	100	87.631
4	Skin permeability (log Kp)	−3.267	−2.968	−3.285
5	P-glycoprotein substrate	Yes	Yes	Yes
6	P-glycoprotein I inhibitor	Yes	Yes	No
7	P-glycoprotein II inhibitor	Yes	No	No

products and may influence formulation strategies; however, low solubility alone does not necessarily preclude good oral absorption.

The Caco-2 permeability values for most compounds were within an acceptable range, suggesting moderate to good intestinal membrane permeability. This indicates that despite low solubility, the ligands are capable of crossing intestinal epithelial barriers effectively.

Predicted human intestinal absorption was high for all compounds, ranging from 85.3% to 100%, demonstrating excellent oral absorption potential. Withanone, Withanolide A, and Withanolide E showed complete (100%) predicted absorption, while Withaferin A and Withanolide F also exhibited strong absorption above 85%.

The skin permeability values (log Kp) were low for all ligands (−2.97 to −3.36), indicating limited transdermal penetration. This suggests that these compounds

are more suitable for oral administration rather than transdermal delivery.

All ligands were predicted to be P-glycoprotein substrates, indicating potential interaction with efflux transporters that may influence absorption and bioavailability. Most compounds were also predicted to inhibit P-glycoprotein I, while inhibition of P-glycoprotein II was observed for Withaferin A, Withanone, Withanolide A, and Withanolide D, but not for Withanolide E and Withanolide F. These interactions may enhance intracellular retention but could also contribute to potential drug-drug interaction risks.

4.7 Distribution Analysis

The distribution-related pharmacokinetic properties of Withaferin A, Withanone, Withanolide A, D, E, and F were predicted using the pkCSM server, and the results are summarized in the Tables 4.13 and 4.14.

TABLE 4.13: Distribution properties of the ligands (Withaferin A, Withanone, and Withanolide A).

Sr. no.	**Characteristic**	**Withaferin A**	**Withanone**	**Withanolide A**
1	VDss (human) (log L/kg)	−0.131	0.081	−0.097
2	Fraction unbound (human) (Fu)	0.105	0.154	0.096
3	BBB permeability (log BB)	−0.03	−0.259	−0.255
4	CNS permeability (log PS)	−2.72	−2.719	−2.681

TABLE 4.14: Distribution properties of the ligands (Withanolide D, Withanolide E, and Withanolide F).

Sr. no.	**Characteristic**	**Withanolide D**	**Withanolide E**	**Withanolide F**
1	VDss (human) (log L/kg)	−0.048	0.093	−0.075
2	Fraction unbound (human) (Fu)	0.093	0.286	0.301
3	BBB permeability (log BB)	−0.315	−0.956	−0.9
4	CNS permeability (log PS)	−2.696	−3.098	−3.108

The predicted volume of distribution at steady state (VDss) for all ligands ranged from −0.131 to 0.093 log L/kg, indicating moderate systemic distribution. These

values suggest that the compounds are likely to be reasonably distributed between plasma and tissues without excessive accumulation in peripheral compartments. The fraction unbound (Fu) values ranged from 0.093 to 0.301, indicating that a portion of each compound remains unbound to plasma proteins and is therefore pharmacologically available. Withanolide E and F exhibited relatively higher unbound fractions, suggesting greater availability for interaction with biological targets compared to the other ligands.

The predicted blood-brain barrier (BBB) permeability (log BB) values were negative for all compounds (−0.03 to −0.96), indicating limited penetration across the blood-brain barrier. This suggests a low likelihood of central nervous system exposure, which may be advantageous for minimizing CNS-related side effects in non-neurological therapeutic applications. Consistent with BBB predictions, the central nervous system (CNS) permeability (log PS) values were also low (−2.68 to −3.11), further confirming restricted CNS distribution. Withanolide E and F showed the lowest CNS permeability, indicating the least potential for central nervous system accumulation.

4.7.1 Metabolism Analysis

The metabolic behavior of Withaferin A, Withanone, Withanolide A, D, E, and F was predicted using the pkCSM server, and the results are presented in the Tables 4.15 and 4.16.

Table 4.15: Metabolism properties of the ligands (Withaferin A, Withanone, and Withanolide A).

Sr. no.	**Characteristic**	**Withaferin A**	**Withanone**	**Withanolide A**
1	CYP2D6 substrate	No	No	No
2	CYP3A4 substrate	Yes	Yes	Yes
3	CYP1A2 inhibitor	No	No	No
4	CYP2C19 inhibitor	No	No	No
5	CYP2C9 inhibitor	No	No	No
6	CYP2D6 inhibitor	No	No	No
7	CYP3A4 inhibitor	No	No	No

TABLE 4.16: Metabolism properties of the ligands (Withanolide D, Withanolide E, and Withanolide F).

Sr. no.	**Characteristic**	**Withanolide D**	**Withanolide E**	**Withanolide F**
1	CYP2D6 substrate	No	No	No
2	CYP3A4 substrate	Yes	Yes	Yes
3	CYP1A2 inhibitor	No	No	No
4	CYP2C19 inhibitor	No	No	No
5	CYP2C9 inhibitor	No	No	No
6	CYP2D6 inhibitor	No	No	No
7	CYP3A4 inhibitor	No	No	No

All six ligands were predicted to be non-substrates of CYP2D6, indicating that this enzyme is unlikely to play a significant role in their metabolic clearance. In contrast, all compounds were identified as substrates of CYP3A4, suggesting that hepatic metabolism via this major cytochrome P450 isoform represents the primary metabolic pathway for these ligands. Importantly, none of the compounds were predicted to inhibit key cytochrome P450 enzymes, including CYP1A2, CYP2C19, CYP2C9, CYP2D6, and CYP3A4. The absence of CYP inhibition indicates a low potential for drug-drug interactions, which is a favorable characteristic for drug development.

4.7.2 Excretion Analysis

The excretion profiles of Withaferin A, Withanone, Withanolide A, D, E, and F were predicted using the pkCSM server, and the results are summarized in the Table 4.17.

TABLE 4.17: Excretion properties of the ligands.

Sr. no.	**Ligand**	**Total clearance (log ml/min/kg)**	**Renal OCT2 substrate**
1	Withaferin A	0.435	Yes
2	Withanone	0.385	Yes
3	Withanolide A	0.337	Yes
4	Withanolide D	0.347	No
5	Withanolide E	0.378	No
6	Withanolide F	0.489	No

The predicted total clearance values for the six ligands ranged from 0.337 to 0.489 log mL/min/kg, indicating moderate clearance rates. Such values suggest that the compounds are neither rapidly eliminated nor excessively retained in the body, which is favorable for maintaining therapeutic concentrations without frequent dosing.

Withanolide F exhibited the highest predicted clearance, suggesting comparatively faster elimination, while Withanolide A showed the lowest clearance, indicating a potentially longer systemic persistence.

The remaining ligands demonstrated comparable clearance values, reflecting similar elimination behavior. Regarding renal excretion, Withaferin A, Withanone, and Withanolide A were predicted to be substrates of the renal organic cation transporter 2 (OCT2), suggesting partial renal involvement in their elimination.

In contrast, Withanolide D, E, and F were predicted not to be OCT2 substrates, indicating that their clearance is likely dominated by non-renal pathways, such as hepatic metabolism.

4.7.3 Toxicity Analysis

The toxicity profiles of Withaferin A, Withanone, Withanolide A, D, E, and F were predicted using the pkCSM server, and the results are summarized in the Tables 4.18 and 4.19.

All six ligands were predicted to be non-mutagenic, as indicated by negative AMES toxicity results, suggesting a low risk of genotoxicity. In addition, none of the compounds were identified as hERG I or hERG II inhibitors, indicating a minimal likelihood of cardiotoxicity associated with QT interval prolongation.

The predicted maximum tolerated dose (MTD) values ranged from -1.093 to -0.613 log mg/kg/day, reflecting acceptable human tolerance levels. Withanolide F exhibited the highest MTD value, suggesting comparatively better tolerability among the evaluated compounds.

The acute oral toxicity (LD_{50}) values for rats ranged from 2.49 to 3.50 mol/kg, indicating low acute toxicity across all ligands. Withanolide E showed the highest LD_{50} value, suggesting the lowest acute toxicity, whereas Withanolide F demonstrated relatively higher acute toxicity compared to the other compounds. Chronic toxicity predictions, represented by LOAEL values, ranged from 0.918 to 2.154 log mg/kg bw/day, indicating that adverse effects are expected only at relatively higher doses. Withaferin A exhibited the lowest LOAEL value, suggesting a comparatively narrower chronic safety margin.

All compounds were predicted to be non-hepatotoxic and non-skin sensitizing, further supporting their favorable safety profiles. Environmental toxicity predictions, including T. pyriformis and Minnow toxicity, showed moderate values, indicating manageable ecological risk.

TABLE 4.18: Toxicity properties of the ligands (Withaferin A, Withanone, and Withanolide A).

Sr. no.	**Characteristic**	**Withaferin A**	**Withanone**	**Withanolide A**
1	AMES toxicity	No	No	No
2	Max. tolerated dose (human) (log mg/kg/day)	−0.695	−1.093	−0.967
3	hERG I inhibitor	No	No	No
4	hERG II inhibitor	No	No	No
5	Oral rat acute toxicity (LD_{50}) (mol/kg)	2.779	2.907	2.913
6	Oral rat chronic toxicity (LOAEL) (log mg/kg_bw/day)	0.918	1.676	1.739
7	Hepatotoxicity	No	No	No
8	Skin sensitisation	No	No	No
9	*T. pyriformis* toxicity	0.299	0.299	0.298
10	Minnow toxicity	0.738	1.322	1.22

4.8 Lead Compound Identification

All six ligands comply with Lipinski's Rule of Five, exhibiting acceptable molecular weight (¡ 500 Da), log P values within the recommended range, and permissible numbers of hydrogen bond donors and acceptors. This confirms that

TABLE 4.19: Toxicity properties of the ligands (Withanolide D, Withanolide E, and Withanolide F).

Sr. no.	**Characteristic**	**Withanolide D**	**Withanolide E**	**Withanolide F**
1	AMES toxicity	No	No	No
2	Max. tolerated dose (human) (log mg/kg/day)	−0.867	−0.768	−0.613
3	hERG I inhibitor	No	No	No
4	hERG II inhibitor	No	No	No
5	Oral rat acute toxicity (LD_{50}) (mol/kg)	2.831	3.503	2.494
6	Oral rat chronic toxicity (LOAEL) (log mg/kg_bw/day)	1.776	2.154	2.122
7	Hepatotoxicity	No	No	No
8	Skin sensitisation	No	No	No
9	*T. pyriformis* toxicity	0.305	0.286	0.286
10	Minnow toxicity	1.178	2.578	2.725

none of the compounds are eliminated at the initial drug-likeness screening stage. However, when ADMET properties are considered collectively to differentiate the most promising candidate, Withanolide E demonstrates the most favorable overall balance:

i. Absorption Withanolide E shows 100% predicted human intestinal absorption, along with acceptable Caco-2 permeability, supporting strong oral bioavailability.

ii. Distribution It exhibits a higher fraction unbound (Fu) compared to most other ligands and limited BBB and CNS penetration, which is advantageous for reducing central nervous system-related side effects in non-CNS targets.

iii. Metabolism Like the other ligands, Withanolide E is a CYP3A4 substrate but does not inhibit any major CYP enzymes, indicating predictable metabolism and a low risk of drug-drug interactions.

iv. Excretion The compound shows moderate total clearance and is not a renal OCT2 substrate, suggesting balanced elimination without excessive renal burden.

v. Toxicity Withanolide E exhibits the highest LD_{50} , higher LOAEL values, and acceptable maximum tolerated dose, indicating a wider safety margin compared to the other compounds. It is also non-mutagenic, non-cardiotoxic, non-hepatotoxic, and non-sensitizing.

4.9 Drug Selection

Although KEGG Disease analysis identified zanidatamab, pembrolizumab, and durvalumab as therapeutic agents for gallbladder cancer, these drugs are monoclonal antibody-based biologics. Due to their large molecular size and proteinaceous nature, conventional molecular docking and ADMET prediction tools are not applicable.

Therefore, these drugs were used as clinical reference standards, while Ashwagandha-derived phytochemicals were evaluated through structure-based molecular docking and pharmacokinetic analysis.

In addition, gemcitabine, a clinically used small-molecule chemotherapeutic agent for gallbladder cancer, was selected as a reference compound for comparative molecular docking and ADMET evaluation.

4.9.1 Gemcitabine

Gemcitabine treats gallbladder cancer by inhibiting tumor progression and prolonging survival. The mechanism involves inhibiting cell proliferation and inducing apoptosis (programmed cell death) in the gallbladder cancer cells [70]. The three-dimensional (3D) structure of gemcitabine was downloaded from PubChem, as shown in Figure 4.10.

The chemical and structural details of gemcitabine retrieved from PubChem are presented in Table 4.20.

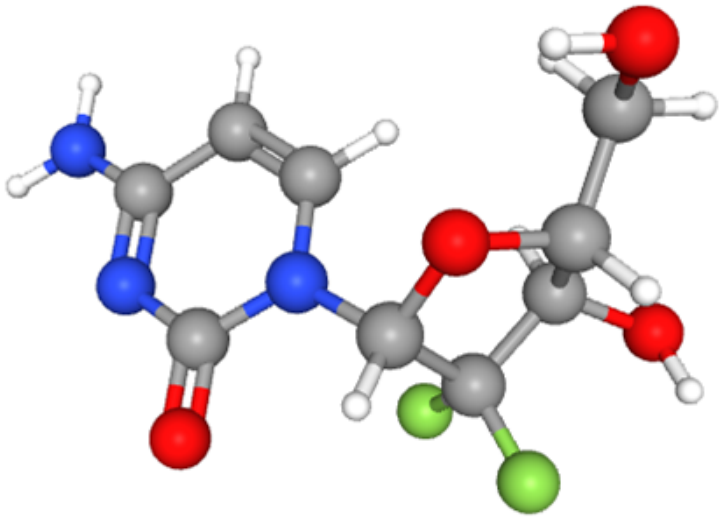

FIGURE 4.10: 3D structure of Gemcitabine (PubChem)

TABLE 4.20: Chemical and structural information of gemcitabine (PubChem).

Sr. no.	**Property**	**Value**
1	Drug	Gemcitabine
2	PubChem CID	60750
3	Molecular formula	$C_9H_{11}F_2N_3O_4$
4	Molecular weight	263.20 g/mol
5	Rotatable bond count	2

4.9.2 Mechanism of Action of Gemcitabine

Gemcitabine is a pyrimidine nucleoside analog that exerts its anticancer effects by disrupting DNA synthesis and cell-cycle progression, leading to tumor cell death. Its activity is S-phase-specific and occurs through two complementary mechanisms [71]:

i. Intracellular Activation

After entering the cell via nucleoside transporters, gemcitabine is phosphorylated by deoxycytidine kinase to its active metabolites [72]:

(a) gemcitabine diphosphate (*dFdCDP*)

(b) gemcitabine triphosphate (*dFdCTP*)

ii. Inhibition of Ribonucleotide Reductase (RNR)

Gemcitabine diphosphate inhibits RNR, the enzyme responsible for converting ribonucleotides to deoxyribonucleotides. This depletes the cellular pool of deoxynucleotides required for DNA replication, stalling DNA synthesis [73].

iii. Incorporation into DNA and Chain Termination

Gemcitabine diphosphate competes with deoxycytidine triphosphate for incorporation into growing DNA strands. Once incorporated, gemcitabine causes "masked chain termination": one additional nucleotide can be added, but further elongation is blocked. This prevents DNA repair enzymes from recognizing and removing the analog, making the damage persistent [72].

iv. Induction of apoptosis

The combined effects of nucleotide depletion and irreparable DNA damage activate DNA damage response pathways. This leads to cell-cycle arrest and apoptosis, often involving TP53-dependent or TP53-independent signaling [72].

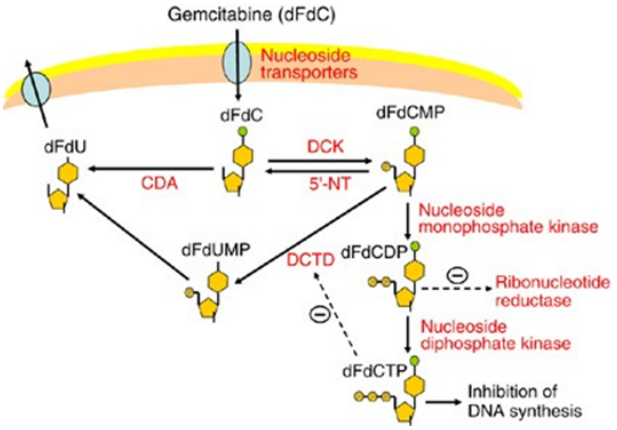

FIGURE 4.11: Cellular Metabolism and Mechanism of Gemcitabine [74]

As illustrated in Figure 4.11, gemcitabine undergoes intracellular uptake through nucleoside transporters and is subsequently activated by phosphorylation via deoxycytidine kinase (dCK) to form its active metabolites. These metabolites inhibit ribonucleotide reductase and DNA synthesis, leading to depletion of deoxynucleotide pools and incorporation into DNA. The resulting replication stress

and irreparable DNA damage trigger DNA damage response pathways, ultimately causing cell-cycle arrest and induction of apoptosis through TP53-dependent or TP53-independent mechanisms [74].

4.9.3 Effects of Gemcitabine on Body

Gemcitabine is a deoxycytidine nucleoside analog that has become a cornerstone chemotherapeutic agent in the treatment of various solid tumors due to its ability to disrupt DNA synthesis and induce apoptosis in rapidly dividing cancer cells. Its clinical application extends beyond traditional cytotoxicity, with emerging evidence highlighting its complex interactions within the tumor microenvironment and potential immunomodulatory roles.

Despite its therapeutic benefits, gemcitabine's use is often limited by the development of drug resistance and a spectrum of adverse effects, including hematological toxicities such as neutropenia and thrombocytopenia, gastrointestinal disturbances, and vascular or pulmonary complications, which necessitate careful monitoring during treatment.

Recent studies continue to explore both the molecular mechanisms underlying gemcitabine's action and strategies to optimize its clinical efficacy while managing toxicity [75].

4.9.3.1 Hematological Toxicity

Gemcitabine commonly causes bone marrow suppression, leading to hematologic toxicities such as neutropenia, thrombocytopenia, and anemia. These are frequently observed adverse events in clinical practice and can affect treatment tolerability and patient outcomes. Clinical data from patients with advanced biliary tract cancers treated with gemcitabine-based regimens report anemia (23%), thrombocytopenia (15-16%), and neutropenia (10%) as common treatment-related adverse even [76].

4.9.3.2 Gastrointestinal Side Effects

Gemcitabine also causes gastrointestinal side effects including nausea and vomiting. These are often grade 1-2 events but may impact quality of life and require supportive management in patients undergoing chemotherapy [77].

4.9.3.3 Fatigue and Constitutional Symptoms

Fatigue and general weakness are commonly reported in patients receiving gemcitabine, reflecting its systemic impact beyond tumor control [77].

4.9.3.4 Pulmonary Toxicity

Pulmonary adverse effects, although less common, have been observed in patients treated with gemcitabine. Reports indicate that dyspnoea and other pulmonary issues may occur, and these toxicities can vary in severity depending on patient susceptibility [78].

4.9.3.5 Rare Vascular and Microangiopathic Events

Case reports and clinical observations have described rare but serious complications such as thrombotic microangiopathy and related organ injury in patients receiving prolonged gemcitabine treatment, underscoring the need for careful monitoring in susceptible individuals [79].

4.9.3.6 Combination Therapy Adverse Events

In real-world studies evaluating gemcitabine combined with cisplatin and immunotherapy (e.g., durvalumab), grade 1-2 adverse events such as anemia, thrombocytopenia, neutropenia, nausea, and fatigue were documented, and more severe (grade 3-4) hematologic toxicities occurred but were less frequent [75].

4.9.4 Physicochemical Properties of Gemcitabine

Information related to drug was retrieved through, pkCSM tool (http://biosig.unimelb.edu.au/pkcsm/). Four of these properties are used for calculation of Lipinski's Rule of Five as shown in the Table 4.21.

TABLE 4.21: Physicochemical properties (Lipinski's Ro5) of gemcitabine.

Sr. no.	**Property**	**Value**
1	Molecular weight	263.2
2	Log P value	−1.2886
3	H-bond donor	3
4	H-bond acceptor	7
5	Rotatable bonds	2

4.9.5 ADMET Profiling of Gemcitabine

When a drug is administrated into the body, it undergoes various systematic steps as it gets absorbed, distributed through the body, metabolized and then excreted (ADME). pkCSM tool (http://biosig.unimelb.edu.au/pkcsm/) was used for ADMET properties of drug.

4.9.6 Adsorption Analysis

As shown in the Table 4.22, the pkCSM absorption analysis of gemcitabine indicates moderate aqueous solubility (−2.749 log mol/L) but low Caco-2 permeability, reflecting its polar nature and limited passive membrane diffusion. The predicted human intestinal absorption of 68.49% suggests moderate oral uptake, consistent with its clinical administration via the intravenous route. Low skin permeability further supports its unsuitability for transdermal delivery. Additionally, gemcitabine is neither a substrate nor an inhibitor of P-glycoprotein, indicating minimal involvement of efflux transporters in its absorption.

TABLE 4.22: Adsorption properties of gemcitabine.

Sr. no.	Property	Value
1	Water solubility (log mol/L)	−2.749
2	Caco2 permeability (log Papp in 10^{-6} cm/s)	−0.053
3	Intestinal absorption (human) (%)	68.491
4	Skin permeability (log Kp)	−2.81
5	P-glycoprotein substrate	No
6	P-glycoprotein I inhibitor	No
7	P-glycoprotein II inhibitor	No

4.9.6.1 Distribution Analysis

The predicted distribution profile of gemcitabine indicates a low volume of distribution (VDss = −0.283 log L/kg), as shown in Table 4.23, suggesting limited tissue penetration and predominant retention within the plasma compartment. The high fraction unbound value (Fu = 0.788) reflects minimal plasma protein binding, allowing a substantial proportion of free drug to remain pharmacologically active. The negative blood-brain barrier permeability (log BB = −0.878) and low central nervous system permeability (log PS = −3.61) indicate poor penetration into the brain, reducing the likelihood of central nervous system-related side effects.

TABLE 4.23: Distribution properties of gemcitabine.

Sr. no.	Property	Value
1	VDss (human) (log L/kg)	−0.283
2	Fraction unbound (human) (Fu)	0.788
3	BBB permeability (log BB)	−0.878
4	CNS permeability (log PS)	−3.61

4.9.6.2 Metabolism Analysis

As shown in the Table 4.24, the pkCSM metabolism analysis indicates that gemcitabine is neither a substrate nor an inhibitor of major cytochrome P450 enzymes, including CYP2D6 and CYP3A4. Additionally, it does not inhibit CYP1A2,

CYP2C9, CYP2C19, or CYP2D6. This suggests that gemcitabine undergoes minimal CYP-mediated hepatic metabolism and possesses a low potential for cytochrome P450-related drug-drug interactions, consistent with its known metabolic activation via non-CYP enzymatic pathways.

TABLE 4.24: Metabolism properties of gemcitabine.

Sr. no.	**Property**	**Value**
1	CYP2D6 substrate	No
2	CYP3A4 substrate	No
3	CYP1A2 inhibitor	No
4	CYP2C19 inhibitor	No
5	CYP2C9 inhibitor	No
6	CYP2D6 inhibitor	No
7	CYP3A4 inhibitor	No

4.10 Excretion Analysis

The predicted excretion profile of gemcitabine shows a moderate total clearance value (0.415 log mL/min/kg), as shown in Table 4.25, indicating balanced elimination without excessive drug accumulation. The compound is not predicted to be a renal OCT2 substrate, suggesting that its clearance is not significantly dependent on OCT2-mediated renal transport and is likely governed by alternative metabolic and elimination pathways.

TABLE 4.25: Excretion properties of gemcitabine.

Sr. no.	**Property**	**Value**
1	Total clearance (log ml/min/kg)	0.415
2	Renal OCT2 substrate	No

4.10.0.1 Toxicity Analysis

The predicted toxicity profile of gemcitabine, as shown in Table 4.26, indicates that it is non-mutagenic, as evidenced by a negative AMES toxicity result, and does not

inhibit hERG I or hERG II channels, suggesting a low potential risk of cardiotoxicity. The predicted maximum tolerated dose (0.182 log mg/kg/day) and oral rat acute toxicity (LD_{50} = 1.959 mol/kg) reflect moderate toxicity consistent with its chemotherapeutic nature. The chronic toxicity value (LOAEL = 2.475 log mg/kg bw/day) suggests that adverse effects occur at relatively higher exposure levels. Gemcitabine is predicted to be hepatotoxic, which aligns with clinically reported liver-related adverse effects, while no skin sensitization is predicted. Environmental toxicity predictions indicate moderate toxicity toward aquatic organisms.

TABLE 4.26: Toxicity properties of gemcitabine.

Sr. no.	**Property**	**Value**
1	AMES toxicity	No
2	Max. tolerated dose (human) (log mg/kg/day)	0.182
3	hERG I inhibitor	No
4	hERG II inhibitor	No
5	Oral rat acute toxicity (LD_{50}) (mol/kg)	1.959
6	Oral rat chronic toxicity (LOAEL) (log mg/kg_bw/day)	2.475
7	Hepatotoxicity	Yes
8	Skin sensitisation	No
9	*T. pyriformis* toxicity	0.275
10	Minnow toxicity	3.531

4.11 Molecular Docking of Gemcitabine and TP53

This section presents the molecular docking analysis of gemcitabine with the TP53 protein to evaluate their binding interactions and potential binding affinity.

4.11.1 Docking Parameters

i. Protein (receptor): TP53

ii. Ligand: Gemcitabine

iii. Scoring function: AutoDock Vina

iv. Grid center: X = 90.428, Y = 89.999, Z = 88.821

v. Grid size: 26 × 26 × 26Å

vi. Grid spacing: 1Å

vii. Exhaustiveness: 8

These parameters are within acceptable limits for reliable docking and ensure adequate sampling of ligand conformations within the selected region.

4.11.2 Docking Results

Molecular docking analysis was performed to evaluate the binding interaction between TP53 and the reference chemotherapeutic agent gemcitabine using AutoDock Vina. The docking results yielded multiple binding poses, as shown in Table 4.27, which were ranked according to their predicted binding affinities. The best binding conformation (Mode 1) exhibited a binding affinity of −9.333

TABLE 4.27: Docking results of TP53 and Gemcitabine

Mode	**Binding Affinity (kcal/mol)**	**Distance from Best Mode**	
		RMSD l.b. (*Å*)	**RMSD u.b.** (*Å*)
1	-9.333	0.000	0.000
2	-9.063	2.200	3.030
3	-9.010	1.725	2.645
4	-8.792	2.630	5.719
5	-8.382	2.501	3.692
6	-8.249	2.943	5.749
7	-8.104	4.199	6.451
8	-7.754	3.181	6.020
9	-7.628	2.708	5.954

kcal/mol, indicating a strong and energetically favorable interaction between gemcitabine and TP53. The root mean square deviation (RMSD) values for this mode

were 0.0 $\AA$, confirming that it represents the most stable and optimal docking pose. Additional binding modes displayed affinities ranging from -9.063 to -7.628 kcal/mol, with increasing RMSD values, suggesting alternative but less favorable orientations of gemcitabine on the TP53 surface. The presence of multiple energetically comparable conformations indicates binding flexibility and supports the plausibility of gemcitabine interacting with TP53 at a surface-accessible region rather than a deeply buried pocket.

Given that TP53 is a tumor suppressor protein and not an enzymatic target, the observed docking interactions are consistent with surface-mediated binding, which may influence protein conformation or regulatory interactions rather than catalytic inhibition. The strong binding affinity observed for gemcitabine supports its role as a reference compound in comparative docking studies with Ashwagandha-derived phytochemicals.

4.12 Gemcitabine and TP53 Interaction

The docked complex, as shown in Figure 4.12, illustrates gemcitabine bound to a surface-accessible region of TP53 rather than a deep binding pocket, which is consistent with the regulatory nature of TP53. The ligand adopts a stable orientation within a shallow groove formed by surrounding TP53 residues and is stabilized by multiple hydrogen-bond and polar interactions. This surface-mediated binding suggests a modulatory interaction that may influence TP53 conformation or regulatory interactions rather than direct enzymatic inhibition, supporting the docking affinity results and validating gemcitabine as a suitable reference compound.

4.13 Comparison of Drug and Lead Compound

Comparison between Gemcitabine and Withanolide E helps to identify the better treatment for Gallbladder Cancer. Comparison is being performed through parameters like: Physiochemical properties, ADMET properties and docking score

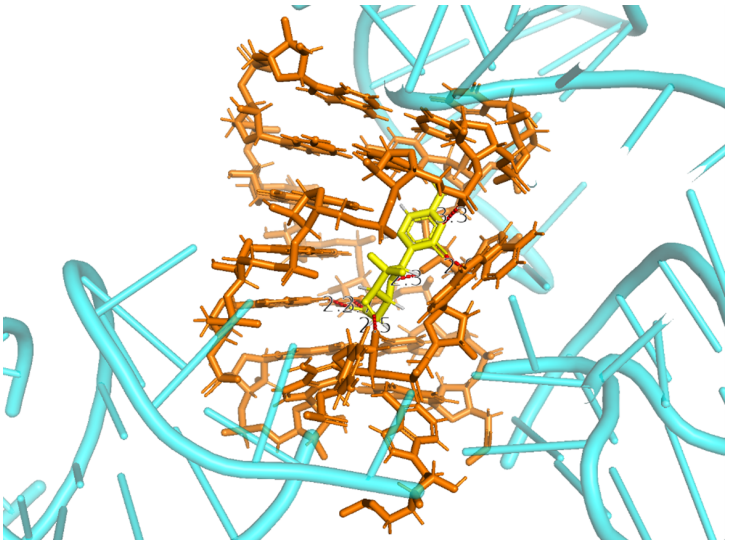

FIGURE 4.12: Interaction of TP53 and Gemcitabine

of Gemcitabine and Withanolide E.

4.13.1 Comparison of Physicochemical Properties

As shown in Table 4.28, the comparison of physicochemical properties reveals notable differences between gemcitabine and withanolide E that may influence their pharmacokinetic behavior.

TABLE 4.28: Comparison of physicochemical properties of gemcitabine and the lead compound.

Sr. no.	**Property**	**Gemcitabine**	**Withanolide E**
1	Molecular weight	263.2	486.605
2	Log P value	−1.2886	2.7544
3	H-bond donor	3	3
4	H-bond acceptor	7	7
5	Rotatable bonds	2	2

Gemcitabine has a substantially lower molecular weight (263.2 Da) compared to withanolide E (486.605 Da), which may favor better diffusion and formulation flexibility. In contrast, withanolide E remains within the acceptable molecular weight limit defined by Lipinski's Rule of Five.

Gemcitabine exhibits a negative log P value (−1.2886), indicating high hydrophilicity, whereas withanolide E shows moderate lipophilicity (log P = 2.7544),

which may enhance membrane permeability. Both compounds possess identical numbers of hydrogen bond donors and acceptors, suggesting comparable hydrogen-bonding capacity and potential for intermolecular interactions. Additionally, the two molecules have the same number of rotatable bonds, indicating similar conformational flexibility. Overall, gemcitabine displays properties associated with high polarity and aqueous solubility, while withanolide E demonstrates a more balanced physicochemical profile that may favor membrane permeability and oral drug-likeness.

4.13.2 Comparison of ADMET Properties

This section presents a comparative evaluation of the ADMET properties of gemcitabine and withanolide E to assess their pharmacokinetic and toxicity profiles.

4.13.2.1 Adsorption

Table 4.29 presents the absorption analysis, which reveals distinct differences between gemcitabine and withanolide E that reflect their contrasting physicochemical characteristics.

TABLE 4.29: Comparison of adsorption properties of gemcitabine and the lead compound.

Sr. no.	**Property**	**Gemcitabine**	**Withanolide E**
1	Water solubility (log mol/L)	−2.749	−5.252
2	Caco2 permeability (log Papp in 10^{-6} cm/s)	−0.053	0.742
3	Intestinal absorption (human) (%)	68.491	100
4	Skin permeability (log Kp)	−2.81	−2.968
5	P-glycoprotein substrate	No	Yes
6	P-glycoprotein I inhibitor	No	Yes
7	P-glycoprotein II inhibitor	No	No

Gemcitabine demonstrates higher aqueous solubility (−2.749 log mol/L) than withanolide E (−5.252 log mol/L), consistent with its hydrophilic nature. However, gemcitabine shows low Caco-2 permeability and moderate predicted human

intestinal absorption (68.49%), indicating limited passive membrane diffusion. In contrast, withanolide E exhibits significantly higher Caco-2 permeability and complete predicted intestinal absorption (100%), suggesting superior membrane permeability and oral absorption potential despite its lower solubility. Both compounds display low skin permeability, indicating limited suitability for transdermal delivery. Withanolide E is predicted to be a P-glycoprotein substrate and inhibitor, which may influence its intestinal transport and bioavailability, whereas gemcitabine shows no interaction with P-glycoprotein. Overall, gemcitabine's absorption profile is characterized by good solubility but limited permeability, whereas withanolide E demonstrates a more favorable balance between permeability and intestinal absorption, supporting its potential as an orally bioavailable compound.

4.13.2.2 Distribution

Table 4.30 presents the distribution analysis, which indicates notable differences between gemcitabine and withanolide E in terms of systemic disposition.

TABLE 4.30: Comparison of distribution properties of gemcitabine and the lead compound.

Sr. no.	**Property**	**Gemcitabine**	**Withanolide E**
1	VDss (human) (log L/kg)	−0.283	0.093
2	Fraction unbound (human) (Fu)	0.788	0.286
3	BBB permeability (log BB)	−0.878	−0.956
4	CNS permeability (log PS)	−3.61	−3.098

Gemcitabine exhibits a lower volume of distribution (VDss = −0.283 log L/kg), suggesting limited tissue penetration and predominant distribution within the plasma compartment. In contrast, withanolide E shows a higher VDss value (0.093 log L/kg), indicating greater tissue distribution.

The fraction unbound in plasma is substantially higher for gemcitabine (Fu = 0.788) than for withanolide E (Fu = 0.286), reflecting weaker plasma protein binding and a larger proportion of freely circulating drug. Both compounds display poor blood-brain barrier permeability and low central nervous system penetration,

as indicated by negative log BB and log PS values, suggesting minimal central nervous system exposure. Overall, gemcitabine demonstrates plasma-restricted distribution with high free-drug availability, whereas withanolide E exhibits enhanced tissue distribution but stronger plasma protein binding.

4.13.2.3 Metabolism

The metabolic analysis, as shown in the Table 4.31, indicates that both gemcitabine and withanolide E are not substrates of CYP2D6 and do not inhibit major cytochrome P450 enzymes, including CYP1A2, CYP2C9, CYP2C19, CYP2D6, and CYP3A4, suggesting a low risk of enzyme-mediated drug-drug interactions. However, withanolide E is predicted to be a substrate of CYP3A4, indicating that its metabolism may primarily occur through this hepatic pathway. In contrast, gemcitabine is not a substrate of CYP3A4, consistent with its known activation via non-CYP enzymatic pathways. Overall, gemcitabine exhibits minimal CYP involvement, while withanolide E shows selective CYP3A4-mediated metabolism without inhibitory effects.

TABLE 4.31: Comparison of metabolism properties of gemcitabine and the lead compound.

Sr. no.	**Property**	**Gemcitabine**	**Withanolide E**
1	CYP2D6 substrate	No	No
2	CYP3A4 substrate	No	Yes
3	CYP1A2 inhibitor	No	No
4	CYP2C19 inhibitor	No	No
5	CYP2C9 inhibitor	No	No
6	CYP2D6 inhibitor	No	No
7	CYP3A4 inhibitor	No	No

4.13.2.4 Excretion

The excretion analysis, as shown in Table 4.32, indicates that both gemcitabine and withanolide E exhibit moderate total clearance values, suggesting balanced elimination without a strong tendency for accumulation. Gemcitabine displays

a slightly higher predicted total clearance (0.415 log mL/min/kg) compared to withanolide E (0.378 log mL/min/kg), suggesting more rapid systemic elimination.

Neither compound is predicted to be a renal OCT2 substrate, indicating that active OCT2-mediated renal transport is unlikely to play a major role in their excretion. Overall, both compounds demonstrate comparable and favorable excretion profiles.

TABLE 4.32: Comparison of excretion properties of gemcitabine and the lead compound.

Sr. no.	**Property**	**Gemcitabine**	**Withanolide E**
1	Total clearance (log ml/min/kg)	0.415	0.378
2	Renal OCT2 substrate	No	No

4.13.2.5 Toxicity

The toxicity analysis, as shown in Table 4.33, indicates that both gemcitabine and withanolide E are non-mutagenic, as evidenced by negative AMES toxicity results, and neither compound inhibits hERG I or hERG II channels, suggesting a low risk of cardiotoxicity.

Gemcitabine shows a higher predicted maximum tolerated dose in humans, whereas withanolide E exhibits a lower value, indicating differences in dose sensitivity. Withanolide E demonstrates a higher oral rat acute toxicity LD_{50} compared to gemcitabine, suggesting lower acute toxicity. Chronic toxicity predictions show comparable LOAEL values for both compounds.

Notably, gemcitabine is predicted to be hepatotoxic, while withanolide E shows no hepatotoxicity, indicating a more favorable hepatic safety profile. Both compounds are predicted to be non-sensitizing to skin. Environmental toxicity predictions suggest lower minnow toxicity for withanolide E compared to gemcitabine. Overall, withanolide E exhibits a comparatively safer toxicity profile than gemcitabine.

TABLE 4.33: Comparison of toxicity properties of gemcitabine and the lead compound.

Sr. no.	**Property**	**Gemcitabine**	**Withanolide E**
1	AMES toxicity	No	No
2	Max. tolerated dose (human) (log mg/kg/day)	0.182	−0.768
3	hERG I inhibitor	No	No
4	hERG II inhibitor	No	No
5	Oral rat acute toxicity (LD_{50}) (mol/kg)	1.959	3.503
6	Oral rat chronic toxicity (LOAEL) (log mg/kg_bw/day)	2.475	2.154
7	Hepatotoxicity	Yes	No
8	Skin sensitisation	No	No
9	*T. pyriformis* toxicity	0.275	0.286
10	Minnow toxicity	3.531	2.578

4.13.3 Comparison of Docking Interactions between TP53 and Selected Compounds

As shown in the Table 4.34, Gemcitabine shows stronger binding to TP53 with a best docking score of −9.333 kcal/mol compared to −8.316 kcal/mol for withanolide E, indicating a more favorable interaction. Both complexes display stable top-ranked poses with RMSD values of 0.0 Å, confirming reliable docking. While gemcitabine exhibits overall higher binding affinity, withanolide E also demonstrates stable and energetically favorable interactions, supporting its potential as a natural lead compound despite slightly weaker binding.

TABLE 4.34: Comparison of docking interactions between TP53 and gemcitabine and Withanolide E.

Sr. no.	**Property**	**Gemcitabine & TP53**	**Withanolide E & TP53**
1	Binding affinity (kcal/mol)	−9.333	−8.316
2	Hydrogen bonds	5	1

In light of the physicochemical properties, ADMET profile, and molecular docking results, withanolide E emerges as the more beneficial compound for TP53 modulation and potential treatment of gallbladder cancer, while gemcitabine remains the stronger clinical reference drug. Gemcitabine shows stronger binding affinity

toward TP53 in docking studies, confirming its robust interaction and validating its role as a standard chemotherapeutic agent. However, its physicochemical and ADMET limitations, including poor membrane permeability, moderate intestinal absorption, intravenous-only administration, and predicted hepatotoxicity, restrict its suitability for long-term or targeted modulation of TP53. In contrast, withanolide E demonstrates a balanced physicochemical profile, satisfying Lipinski's Rule of Five, along with excellent predicted intestinal absorption, higher membrane permeability, favorable tissue distribution, and absence of hepatotoxicity. Although its docking affinity toward TP53 is slightly lower than gemcitabine, it still shows stable and energetically favorable binding, consistent with a regulatory or modulatory interaction rather than cytotoxic inhibition. This aligns well with TP53's role as a tumor suppressor protein. Overall, gemcitabine is more effective as a potent anticancer agent, but withanolide E appears more advantageous for TP53 modulation with a better safety and pharmacokinetic profile. Therefore, withanolide E represents a promising natural lead compound for further experimental validation and potential development as a safer, TP53-modulating therapeutic strategy for gallbladder cancer.

Chapter 5

Conclusion and Recommendations

5.1 Conclusion

The present study employed an integrated computational drug discovery approach to identify potential anti-gallbladder cancer compounds derived from *Withania somnifera*, with a particular focus on TP53 modulation. Gallbladder cancer was selected due to its aggressive nature, late-stage diagnosis, poor survival outcomes, and limited accessibility to effective and affordable therapies, especially in developing regions. TP53 was chosen as the primary molecular target owing to its central role in tumor suppression and frequent mutation in gallbladder cancer pathogenesis. A systematic *in silico* workflow was implemented, including ligand selection through literature mining, protein and ligand preparation, physicochemical evaluation, Lipinski's Rule of Five screening, ADMET profiling, molecular docking, and comparative analysis with a standard chemotherapeutic drug. Six phytoconstituents of *W. somnifera* were evaluated, and their performance was benchmarked against gemcitabine, an FDA-approved drug commonly used in gallbladder cancer treatment. Molecular docking results demonstrated that gemcitabine exhibited the strongest binding affinity toward TP53, validating its established role as a

potent anticancer agent. However, gemcitabine displayed notable limitations, including poor membrane permeability, moderate intestinal absorption, intravenous-only administration, and predicted hepatotoxicity, which restrict its long-term and targeted therapeutic applicability.

In contrast, withanolide E showed stable and energetically favorable binding to a surface-accessible region of TP53, consistent with the protein's regulatory and allosteric nature. Importantly, withanolide E satisfied all criteria of Lipinski's Rule of Five and exhibited an excellent ADMET profile, including high predicted intestinal absorption, favorable membrane permeability, balanced tissue distribution, moderate clearance, and absence of hepatotoxicity.

Although its docking affinity was slightly lower than that of gemcitabine, the overall pharmacokinetic and safety advantages of withanolide E suggest its suitability as a TP53-modulating agent rather than a purely cytotoxic compound. In conclusion, while gemcitabine remains the more potent clinical anticancer agent, withanolide E emerges as a promising natural lead compound with superior safety and pharmacokinetic characteristics for TP53 modulation in gallbladder cancer. This study provides a strong computational foundation for further in vitro and in vivo validation of withanolide E and supports its potential development as a safer, plant-derived therapeutic alternative for gallbladder cancer management.

5.2 Recommendations

Based on the findings of the present computational study, several recommendations are proposed to guide future research and facilitate the translational potential of the identified lead compound.

The promising *in silico* results obtained for withanolide E warrant further experimental validation. *In vitro* studies using gallbladder cancer cell lines should be conducted to evaluate its cytotoxicity, TP53 modulation, apoptosis induction, and cell-cycle effects. These experiments would confirm the biological relevance of the predicted computational interactions.

To establish therapeutic potential and safety, *in vivo* studies using appropriate animal models of gallbladder cancer are recommended. These studies should focus on pharmacokinetics, bioavailability, dose optimization, toxicity profiling, and overall antitumor efficacy of withanolide E.

Future work should include molecular dynamics simulations to assess the stability, flexibility, and time-dependent behavior of the TP53-withanolide E complex. This would provide deeper insights into the dynamic nature of binding and confirm the stability of the predicted docking interactions under physiological conditions.

Structural optimization of withanolide E through structure-activity relationship studies may further enhance its binding affinity, selectivity, and pharmacokinetic properties. Semi-synthetic or chemically modified derivatives could be explored to improve therapeutic efficacy.

Given the clinical relevance of gemcitabine, combination studies involving withanolide E and standard chemotherapeutic agents should be investigated. Such combinations may enhance therapeutic outcomes, reduce required drug doses, and potentially mitigate adverse effects.

Although TP53 was selected as the primary target, future studies may explore additional gallbladder cancer-related targets and signaling pathways, such as PI3K/AKT, EGFR, and KRAS, to evaluate the multi-target potential of withanolide E.

If validated experimentally, formulation development and drug delivery strategies should be explored to improve the solubility, stability, and bioavailability of withanolide E, facilitating its progression toward clinical application.

Bibliography

[1] H. Elimam, N. A. A. Alhamshry, A. Hatawsh *et al.*, "Natural products and long noncoding RNA signatures in gallbladder cancer: a review focuses on pathogenesis, diagnosis, and drug resistance," *Naunyn-Schmiedeberg's Archives of Pharmacology*, vol. 397, no. 12, pp. 9549–9571, 2024. [Online]. Available: https://doi.org/10.1007/s00210-024-03279-1

[2] C. T. Marcinak and D. E. Abbott, "Gallbladder cancer," in *Cancer Treatment and Research*. Springer, 2024, pp. 147–163. [Online]. Available: https://doi.org/10.1007/978-3-031-61238-1_8

[3] M. Piñeros, J. Vignat, M. Colombet *et al.*, "Global variations in gallbladder cancer incidence: What do recorded data and national estimates tell us?" *International Journal of Cancer*, vol. 156, no. 7, pp. 1358–1368, 2024. [Online]. Available: https://doi.org/10.1002/ijc.35232

[4] K. Okumura *et al.*, "Gallbladder cancer: Historical treatment and new management options," *World Journal of Gastrointestinal Oncology*, vol. 13, no. 10, pp. 1317–1335, 2021. [Online]. Available: https://doi.org/10.4251/wjgo.v13.i10.1317

[5] Y. Zhou, K. Yuan, Y. Yang *et al.*, "Gallbladder cancer: current and future treatment options," *Frontiers in Pharmacology*, vol. 14, p. 1183619, 2023. [Online]. Available: https://doi.org/10.3389/fphar.2023.1183619

[6] S. Gezici and N. Şekeroğlu, "Current perspectives in the application of medicinal plants against cancer: novel therapeutic agents," *Anti-Cancer Agents in Medicinal Chemistry*, vol. 19, 2018, title normalized from

provided template-like text. [Online]. Available: https://doi.org/10.2174/1871520619666181224121004

[7] K. Patel and D. K. Patel, "Therapeutic role of phytochemicals in gallbladder cancer: Pharmacological activity and associated molecular mechanisms," *Journal of Enterocolitis*, vol. 4, pp. 1–8, 2025. [Online]. Available: https://doi.org/10.14744/jenterocolitis.2025.79495

[8] E. M. Elzayat, G. E. Elsamahy, G. H. Mansour, A. A. El-Sherif, and N. Hassan, "The synergistic and anticancer potential of withania somnifera (ashwagandha) ethanol extract as an adjuvant with doxorubicin in MCF7 breast cancer cell line," *Asian Pacific Journal of Cancer Prevention*, vol. 26, no. 3, pp. 757–766, 2025. [Online]. Available: https://doi.org/10.31557/APJCP.2025.26.3.757

[9] C. Chai *et al.*, "Establishment and characterization of a novel human gallbladder cancer cell line, gbc-x1," *Scientific Reports*, vol. 14, no. 1, pp. 21 439–21 439, Sep. 2024. [Online]. Available: https://doi.org/10.1038/s41598-024-72830-0

[10] S. Vuthaluru, P. Sharma, S. Chowdhury, and C. Are, "Global epidemiological trends and variations in the burden of gallbladder cancer," *Journal of Surgical Oncology*, vol. 128, no. 6, pp. 980–988, 2023. [Online]. Available: https://doi.org/10.1002/jso.27450

[11] H. Guo, D. Zhang, Z. Li, S. Liu, and R. Wang, "Global burden of gallbladder cancer in 2022 and predictions to 2042," *Digestive and Liver Disease*, vol. 57, no. 6, pp. 1294–1300, 2025. [Online]. Available: https://doi.org/10.1016/j.dld.2025.02.007

[12] N. Ahmed, S. Misbah, M. A. Baig, S. Zaidi, and S. M. Ahsan, "Patho-epidemiology of gallbladder lesions; a 5-year study at dow medical college, karachi," *Annals of Jinnah Sindh Medical University*, April 2022, available on ResearchGate. [Online]. Available: https://www.researchgate.net/publication/

360065138_PATHO-EPIDEMIOLOGY_OF_GALLBLADDER_LESIONS_A_5-YEAR_STUDY_AT_DOW_MEDICAL_COLLEGE_KARACHI

[13] A. M. Lucchese, M. C. Machry, A. N. Kalil, A. F. Oliveira, and F. J. F. Coimbra, "Exploring anatomy, macroscopic and microscopic structures, and physiological functions of the gallbladder," in *Gallbladder Cancer*. Springer, 2024, pp. 1–13. [Online]. Available: https://doi.org/10.1007/978-3-031-76746-3_1

[14] M. W. Jones, J. G. Deppen, K. Small, and S. Kashyap, "Physiology, gallbladder," StatPearls [Internet]. Treasure Island (FL): StatPearls Publishing, 2020, accessed 2025-11-02. [Online]. Available: https://www.ncbi.nlm.nih.gov/books/NBK482488/

[15] H. Bhosale, R. Shah, R. Morani, R. Waters, and M. Virarkar, "Gallbladder neuroendocrine neoplasms: a review," *Abdominal Radiology*, pp. 1–12, 2025. [Online]. Available: https://doi.org/10.1007/s00261-025-05204-3

[16] M. Chhabra *et al.*, "Proposal for a new morphological 'combined type' of gallbladder cancer: description of radiopathological characteristics and comparison with other morphological types," *Abdominal Radiology*, vol. 49, no. 3, pp. 703–709, 2023. [Online]. Available: https://doi.org/10.1007/s00261-023-04090-x

[17] A. Al Omran, A. M. Alkhalifa, A. S. Alqattan, and A. A. Alshahrani, "Gallbladder cancer of two histological origins: A case report and review of literature," *International Journal of Surgery Case Reports*, vol. 81, p. 105704, 2021. [Online]. Available: https://doi.org/10.1016/j.ijscr.2021.105704

[18] S. A. Halaseh, S. Halaseh, and R. Shakman, "A review of the etiology and epidemiology of gallbladder cancer: What you need to know," *Cureus*, 2022. [Online]. Available: https://doi.org/10.7759/cureus.28260

[19] P. Pérez-Moreno, I. Riquelme, P. García, P. Brebi, and J. C. Roa, "Environmental and lifestyle risk factors in the carcinogenesis of gallbladder

cancer," *Journal of Personalized Medicine*, vol. 12, no. 2, p. 234, 2022. [Online]. Available: https://doi.org/10.3390/jpm12020234

[20] N. Husain, S. Shukla, and P. Srivastava, "Tumors and tumor-like lesions of the gall bladder—a review," *Indian Journal of Pathology and Microbiology*, vol. 68, no. 4, pp. 676–691, Oct. 2025. [Online]. Available: https://doi.org/10.4103/ijpm.ijpm_649_25

[21] A. Chaturvedi, V. Kumar, and S. Gupta, "Molecular oncology of gall bladder cancer," *Indian Journal of Surgical Oncology*, vol. 12, no. S1, pp. 57–64, 2019. [Online]. Available: https://doi.org/10.1007/s13193-019-01008-2

[22] I. I. Wistuba and J. Albores-Saavedra, "Epigenetic inactivation of tumor suppressor genes in gallbladder carcinoma," *Modern Pathology*, vol. 17, no. 2, pp. 221–230, 2004. [Online]. Available: https://doi.org/10.1038/modpathol.3800045

[23] K. Sugiyama, H. Tazawa, and T. Ohta, "KRAS gene mutations in gallbladder carcinoma with an anomalous junction of the pancreaticobiliary duct," *Cancer*, vol. 82, no. 1, pp. 60–67, 1998.

[24] H. Watanabe, K. Tashiro, and M. Tsuchiya, "Genetic and clinicopathological features of gallbladder carcinoma associated with anomalous pancreaticobiliary duct junction," *Journal of Hepato-Biliary-Pancreatic Surgery*, vol. 15, no. 1, pp. 13–21, 2008. [Online]. Available: https://doi.org/10.1007/s00534-007-1278-0

[25] N. Shukla, M. Tewari, and H. Kumar, "Molecular alterations in gallbladder cancer: A review," *European Journal of Surgical Oncology*, vol. 44, no. 5, pp. 605–614, 2018. [Online]. Available: https://doi.org/10.1016/j.ejso.2018.02.002

[26] J. Singh, D. Shukla, S. Gupta, B. R. Shrivastav, and P. K. Tiwari, "Clinical epidemiology of gallbladder cancer in north-central india and association of immunological markers, NLR, MLR and PLR in the diagnostic/prognostic prediction of GBC," *Cancer Treatment and*

Research Communications, vol. 28, p. 100431, 2021. [Online]. Available: https://doi.org/10.1016/j.ctarc.2021.100431

[27] S. Xu and M. Xu, "Advances in diagnosis and treatment of gallbladder cancer: Current status and future directions," *World Journal of Gastrointestinal Oncology*, vol. 17, no. 5, 2025. [Online]. Available: https://doi.org/10.4251/wjgo.v17.i5.104957

[28] M. Marrelli, "Medicinal plants," *Plants*, vol. 10, no. 7, p. 1355, 2021. [Online]. Available: https://doi.org/10.3390/plants10071355

[29] D. Das, *Medicinal and Aromatic Plants In and Around Protected Areas of the Indian Subcontinent*. Shashwat Publication, Jul. 2024, google Books. Accessed 2025-11-02. [Online]. Available: https://books.google.com.pk/books?hl=en&lr=&id=ndwUEQAAQBAJ

[30] Y. O. Ali Abdalla *et al.*, "Natural products for cancer therapy: A review of their mechanism of actions and toxicity in the past decade," *Journal of Tropical Medicine*, vol. 2022, pp. 1–20, 2022. [Online]. Available: https://doi.org/10.1155/2022/5794350

[31] W. Chaouki, D. Y. Leger, J. Eljastimi, J.-L. Beneytout, and M. Hmamouchi, "Antiproliferative effect of extracts from aristolochia baetica and origanum compactum on human breast cancer cell line MCF-7," *Pharmaceutical Biology*, vol. 48, no. 3, pp. 269–274, 2010. [Online]. Available: https://doi.org/10.3109/13880200903096588

[32] S. J. Mohammed *et al.*, "Structural characterization, antimicrobial activity, and in vitro cytotoxicity effect of black seed oil," *Evidence-Based Complementary and Alternative Medicine*, vol. 2019, pp. 1–9, 2019. [Online]. Available: https://doi.org/10.1155/2019/6515671

[33] S. J. Lang *et al.*, "Antitumor activity of an artemisia annua herbal preparation and identification of active ingredients," *Phytomedicine*, vol. 62, p. 152962, 2019. [Online]. Available: https://doi.org/10.1016/j.phymed.2019.152962

[34] H. Y. Tan, N. Wang, S.-W. Tsao, Z. Zhang, and Y. Feng, "Suppression of vascular endothelial growth factor via inactivation of eukaryotic elongation factor 2 by alkaloids in coptidis rhizome in hepatocellular carcinoma," *Integrative Cancer Therapies*, vol. 13, no. 5, pp. 425–434, 2014. [Online]. Available: https://doi.org/10.1177/1534735413513635

[35] N. Wang *et al.*, "F-actin reorganization and inactivation of rho signaling pathway involved in the inhibitory effect of coptidis rhizoma on hepatoma cell migration," *Integrative Cancer Therapies*, vol. 9, no. 4, pp. 354–364, 2010. [Online]. Available: https://doi.org/10.1177/1534735410379121

[36] A. Waheed, J. Barker, S. J. Barton, C. P. Owen, S. Ahmed, and M. A. Carew, "A novel steroidal saponin glycoside from fagonia indica induces cell-selective apoptosis or necrosis in cancer cells," *European Journal of Pharmaceutical Sciences*, vol. 47, no. 2, pp. 464–473, 2012. [Online]. Available: https://doi.org/10.1016/j.ejps.2012.07.004

[37] H. J. Eo *et al.*, "Anti-inflammatory and anti-cancer activity of mulberry (morus alba l.) root bark," *BMC Complementary and Alternative Medicine*, vol. 14, no. 1, p. 200, 2014. [Online]. Available: https://doi.org/10.1186/1472-6882-14-200

[38] J.-H. Ryu, S.-J. Lee, M.-J. Kim, J.-H. Shin, S.-K. Kang, K.-M. Cho, and N.-J. Sung, "Antioxidant and anticancer activities of artemisia annua l. and determination of functional compounds," *Journal of the Korean Society of Food Science and Nutrition*, vol. 40, no. 4, pp. 509–516, 2011. [Online]. Available: https://doi.org/10.3746/jkfn.2011.40.4.509

[39] Q. Hu, R. Pan, L. Wang, B. Peng, J. Tang, and X. Liu, "Platycodon grandiflorum induces apoptosis in SKOV3 human ovarian cancer cells through mitochondrial-dependent pathway," *The American Journal of Chinese Medicine*, vol. 38, no. 2, pp. 373–386, 2010. [Online]. Available: https://doi.org/10.1142/S0192415X10007919

[40] A. Kumar, D. Husain, R. K. Lal, S. Singh, V. Singh, and A. K. Gupta, "Genetic diversity and future prospects in withania somnifera (l.) dunal: an assessment based on quantitative traits in different accessions of ashwagandha," *The Nucleus*, vol. 66, no. 2, pp. 151–159, 2023. [Online]. Available: https://doi.org/10.1007/s13237-023-00423-9

[41] Y. Srivastav, S. B. Bind, and A. Srivastav, "Ashwagandha (withania somnifera), taxonomy, pharmacological properties and its role in COVID-19 and extraction process: A comprehensive expansion," *International Journal of Pharmaceutical Sciences*, vol. 2, no. 12, pp. 721–734, 2024. [Online]. Available: https://doi.org/10.5281/zenodo.14296564

[42] M. Nabi and N. Tabassum, "Role of environmental toxicants on neurodegenerative disorders," *Frontiers in Toxicology*, vol. 4, 2022. [Online]. Available: https://doi.org/10.3389/ftox.2022.837579

[43] D. Tewari *et al.*, "Withania somnifera (l.) dunal: Phytochemistry, structure-activity relationship, and anticancer potential," *Phytomedicine*, vol. 98, p. 153949, 2022. [Online]. Available: https://doi.org/10.1016/j.phymed.2022.153949

[44] A. Bashir, M. Nabi, N. Tabassum, S. Afzal, and M. Ayoub, "An updated review on phytochemistry and molecular targets of withania somnifera (l.) dunal (ashwagandha)," *Frontiers in Pharmacology*, vol. 14, 2023. [Online]. Available: https://doi.org/10.3389/fphar.2023.1049334

[45] A. N. Sari *et al.*, "Combination of withaferin-a and CAPE provides superior anticancer potency: Bioinformatics and experimental evidence to their molecular targets and mechanism of action," *Cancers*, vol. 12, no. 5, p. 1160, 2020. [Online]. Available: https://doi.org/10.3390/cancers12051160

[46] V. Kumar, A. Dey, M. B. Hadimani, T. Marcovic, and M. Emerald, "Chemistry and pharmacology of withania somnifera: An update," *TANG [Humanitas Medicine]*, vol. 5, no. 1, pp. 1.1–1.13, 2015. [Online]. Available: https://doi.org/10.5667/tang.2014.0030

[47] S. Siddiqui, S. Sanyal, D. Mukherjee, and M. Dwivedi, "The genetic and epidemiological dimensions of gallbladder cancer: Toward effective therapeutic strategies," *Current Gene Therapy*, vol. 25, 2025. [Online]. Available: https://doi.org/10.2174/0115665232366089250610083533

[48] T. Saha and N. Muhammad, "Signaling pathways and molecular biomarkers in gallbladder cancer: A state-of-the-art review," *Current Tissue Microenvironment Reports*, vol. 6, no. 4, pp. 83–113, 2025. [Online]. Available: https://doi.org/10.1007/s43152-025-00062-z

[49] J. I. J. Ellaway, S. Anyango *et al.*, "Identifying protein conformational states in the protein data bank: Toward unlocking the potential of integrative dynamics studies," *Structural Dynamics*, vol. 11, no. 3, p. 034701, 2024. [Online]. Available: https://doi.org/10.1063/4.0000251

[50] R. Chauhan, J. Bhattacharya, R. Solanki, F. J. Ahmad, B. Alankar, and H. Kaur, "Gud-ve visualization tool for physicochemical properties of proteins," *MethodsX*, vol. 10, p. 102226, 2023. [Online]. Available: https://doi.org/10.1016/j.mex.2023.102226

[51] P. Mirzavand Borujeni and R. Salavati, "Functional domain annotation by structural similarity," *NAR Genomics and Bioinformatics*, vol. 6, no. 1, p. lqae005, 2024. [Online]. Available: https://doi.org/10.1093/nargab/lqae005

[52] M. Mihăşan, "What in silico molecular docking can do for the 'bench-working biologists,'," *Journal of Biosciences*, vol. 37, no. S1, pp. 1089–1095, 2012. [Online]. Available: https://doi.org/10.1007/s12038-012-9273-8

[53] G. Henrique, A. Caminero, and R. L. Calil, "Absorption matters: a closer look at popular oral bioavailability rules for drug approvals," *Molecular Informatics*, vol. 42, no. 11, 2023. [Online]. Available: https://doi.org/10.1002/minf.202300115

[54] D. E. V. Pires, T. L. Blundell, and D. B. Ascher, "pkcsm: predicting small-molecule pharmacokinetic and toxicity properties using graph-based

signatures," *Journal of Medicinal Chemistry*, vol. 58, no. 9, pp. 4066–4072, 2015. [Online]. Available: https://doi.org/10.1021/acs.jmedchem.5b00104

[55] S. Agnihotry, R. K. Pathak, D. B. Singh, A. Tiwari, and I. Hussain, "Protein structure prediction," in *Bioinformatics*. Elsevier, 2022, pp. 177–188. [Online]. Available: https://doi.org/10.1016/B978-0-323-89775-4.00023-7

[56] A. M. Davis and P. D. Leeson, "Physicochemical properties," in *The Royal Society of Chemistry eBooks*. Royal Society of Chemistry, 2023, pp. 1–39. [Online]. Available: https://doi.org/10.1039/9781788018982-00001

[57] D. G. Gamage, A. Gunaratne, G. R. Periyannan, and T. G. Russell, "Applicability of instability index for in vitro protein stability prediction," *Protein and Peptide Letters*, vol. 26, no. 5, pp. 339–347, 2019. [Online]. Available: https://doi.org/10.2174/0929866526666190228144219

[58] A. A. Tokmakov, A. Kurotani, and K.-I. Sato, "Protein pi and intracellular localization," *Frontiers in Molecular Biosciences*, vol. 8, p. 775736, 2021. [Online]. Available: https://doi.org/10.3389/fmolb.2021.775736

[59] E. Gasteiger *et al.*, "Protein identification and analysis tools on the ExPASy server," in *The Proteomics Protocols Handbook*. Humana Press, 2005, pp. 571–607, duplicate entry as provided in source list.

[60] L. Zhang, J. Xie, X. E. Wang, X. Liu, X. Tang, R. Cao, and S. Liang, "Proteomic analysis of mouse liver plasma membrane: use of differential extraction to enrich hydrophobic membrane proteins," *Proteomics*, vol. 5, no. 17, pp. 4510–4524, 2005.

[61] X. Zhou *et al.*, "I-TASSER-MTD: a deep-learning-based platform for multi-domain protein structure and function prediction," *Nature Protocols*, pp. 1–28, 2022. [Online]. Available: https://doi.org/10.1038/s41596-022-00728-0

[62] X.-Y. Meng, H.-X. Zhang, M. Mezei, and M. Cui, "Molecular docking: A powerful approach for structure-based drug discovery," *Current Computer-Aided Drug Design*, vol. 7, no. 2, pp. 146–157, Jun 2011.

[63] D. Sundar *et al.*, "Wild type p53 function in p53y220c mutant harboring cells by treatment with ashwagandha derived anticancer withanolides: bioinformatics and experimental evidence," *Journal of Experimental & Clinical Cancer Research*, vol. 38, no. 1, Feb 2019. [Online]. Available: https://doi.org/10.1186/s13046-019-1099-x

[64] S. R. Regmi, N. P. Sawd, N. H. Khan, and P. R. Joshi, "In silico molecular docking and dynamic study of mdm2-p53 inhibitor alkaloids extracted from withania somnifera against tumor growth," *KMC Journal*, vol. 6, no. 2, pp. 273–297, Aug 2024. [Online]. Available: https://doi.org/10.3126/kmcj.v6i2.68906

[65] X. Chen, X. Ma, X. Hu, C. Wang, X. Zhang, and C. Yan, "Mechanisms and potential therapeutic strategies of withaferin a in breast cancer," *Pharmacological Reports*, May 2025.

[66] Q. Tabassam, T. Mehmood, A. R. Raza, A. Ullah, F. Saeed, and F. M. Anjum, "Synthesis, characterization and anti-cancer therapeutic potential of withanolide-a with 20 nm saunps conjugates against skbr3 breast cancer cell line," *International Journal of Nanomedicine*, vol. 15, pp. 6649–6658, Sep 2020.

[67] C. J. Henrich *et al.*, "Withanolide e sensitizes renal carcinoma cells to trail-induced apoptosis by increasing cflip degradation," *Cell Death & Disease*, vol. 6, no. 2, pp. e1666–e1666, Feb 2015.

[68] W. Ben Bakrim *et al.*, "Bioactive metabolites from the leaves of withania adpressa," *Pharmaceutical Biology*, vol. 56, no. 1, pp. 505–510, Jan 2018.

[69] S. Nhlapho *et al.*, "Druggability of pharmaceutical compounds using lipinski rules with machine learning," *Sciences of Pharmacy*, vol. 3, no. 4, 2024. [Online]. Available: https://doi.org/10.58920/sciphar0304264

[70] U. A. Çevik, A. Işik, and A. Karakaya, "ADMET and physicochemical assessments in drug design," in *Computational Methods for Rational*

Drug Design. Wiley, 2024, pp. 123–151. [Online]. Available: https://doi.org/10.1002/9781394249190.ch6

[71] Y. Mita *et al.*, "Antitumor effect of gemcitabine on orthotopically inoculated human gallbladder cancer cells in nude mice," *Annals of Surgical Oncology*, vol. 14, no. 4, pp. 1374–1380, 2007. [Online]. Available: https://doi.org/10.1245/s10434-006-9191-9

[72] W. Plunkett, P. Huang, Y. Z. Xu, V. Heinemann, R. Grunewald, and V. Gandhi, "Gemcitabine: metabolism, mechanisms of action, and self-potentiation," *Seminars in Oncology*, vol. 22, no. 4 Suppl 11, pp. 3–10, 1995. [Online]. Available: https://pubmed.ncbi.nlm.nih.gov/7481842/

[73] W. Plunkett, P. Huang, and V. Gandhi, "Preclinical characteristics of gemcitabine," *Anti-Cancer Drugs*, vol. 6, no. Supplement 6, pp. 7–13, 1995. [Online]. Available: https://doi.org/10.1097/00001813-199512006-00002

[74] H. Ueno, K. Kiyosawa, and N. Kaniwa, "Pharmacogenomics of gemcitabine: can genetic studies lead to tailor-made therapy?" *British Journal of Cancer*, vol. 97, no. 2, pp. 145–151, 2007. [Online]. Available: https://doi.org/10.1038/sj.bjc.6603860

[75] X. Zhang, B. Qi, and J. Chen, "Clinical application and drug resistance mechanism of gemcitabine," *Frontiers in Cell and Developmental Biology*, vol. 13, 2025. [Online]. Available: https://doi.org/10.3389/fcell.2025.1702720

[76] B. Baraka, D. J. Ponda, J. Hanna, D. Gomez, G. Aithal, and A. Arora, "Efficacy and toxicity profile of carboplatin/gemcitabine chemotherapy in locally advanced or metastatic biliary tract cancer: A single UK centre experience," *Cancers*, vol. 17, no. 19, p. 3102, 2025. [Online]. Available: https://doi.org/10.3390/cancers17193102

[77] F. Gerhardt *et al.*, "Treatment with gemcitabine/cisplatin and durvalumab for advanced biliary tract cancer – real-world data from a multicenter german patient population," *Journal of Cancer Research and Clinical*

Oncology, vol. 151, no. 6, 2025. [Online]. Available: https://doi.org/10.1007/s00432-025-06239-1

[78] P. Mouillot *et al.*, "Characteristics and outcomes of gemcitabine-associated pulmonary hypertension," *ERJ Open Research*, vol. 10, no. 3, pp. 00 654–2023, 2024. [Online]. Available: https://doi.org/10.1183/23120541.00654-2023

[79] T. Kuribayashi *et al.*, "Thrombotic microangiopathy associated with gemcitabine in non-small cell lung cancer: A case report," *Case Reports in Oncology*, vol. 14, no. 3, pp. 1712–1718, 2021. [Online]. Available: https://doi.org/10.1159/000520484